

Achievable Rate Analyses and Phase Shift Optimizations on Intelligent Reflecting Surface with Hardware Impairments

Zhe Xing and Rui Wang, *Senior Member, IEEE*

Abstract

Intelligent reflecting surface (IRS) is envisioned as a promising hardware solution to hardware cost and energy consumption in the future fifth-generation (5G) mobile communication network. It exhibits great advantages in enhancing data transmission, but may suffer from performance degradations caused by inherent hardware impairments (HWI), which universally exist in the real-world communication systems. For analysing the achievable rate (ACR) and optimizing the phase shifts in the IRS-aided communication system with HWI, we consider that the HWI appear at both the IRS and the transceivers. By modelling the HWI at the IRS as phase errors and the HWI at the transceivers as distortion noises, we first mathematically derive the closed-form expression of the average ACR with HWI. Then, we formulate optimization problems to optimize the phase shifts of the IRS in the presence of HWI to improve the performance. The solution is obtained by transforming non-convex problems into convex semidefinite programming (SDP) problems. Subsequently, we theoretically compare the average ACR of the IRS-aided system with that of the decode-and-forward (DF) relay assisted system under two different conditions. Extensive simulations are carried out to verify the theoretical analyses. Results demonstrate that the average ACR of the IRS-aided system with HWI is lower than that without HWI, but can exceed that of the DF relay assisted system with HWI when the number of reflecting elements is large enough. It is concluded that the HWI has impact on the IRS, but still leaves opportunities for the IRS to surpass conventional DF relay.

Index Terms

Intelligent reflecting surface (IRS), hardware impairments (HWI), achievable rate (ACR), phase shift optimization, decode-and-forward (DF) relay.

I. INTRODUCTION

The rapid development of the worldwide mobile communication technologies has been witnessed in recent years. After the 4th generation (4G) mobile communications became universal

The authors are with the College of Electronics and Information Engineering, Tongji University, Shanghai 201804, China (e-mail: zxing@tongji.edu.cn; ruiwang@tongji.edu.cn).

Corresponding Author: Rui Wang.

around the world, the initial 5th generation (5G) standard was completed in 2018 and the 5G commercial networks were already employed in part in the first quarter of 2020. For supporting huge mobile data traffic and high-speed communications required by a growing number of mobile devices accessed to the wireless networks, a variety of innovative techniques including millimeter wave (mmWave), ultra-dense network (UDN) and massive multiple-input multiple-output (MIMO) are implemented in 5G wireless transmission systems [1]. These techniques exhibit great advantages in helping the communication systems improve spectral efficiency (SE) [2], but remain challenging problems such as: 1) the mmWave is susceptible to blockage and suffers from serious power attenuation during the long-distance propagation in the atmosphere [3], so that the wireless system will bear poor reliability when the received signals are substantially weak; 2) the UDN is composed of numerous intensively distributed base stations (BS) [4] while the massive MIMO requests the transceivers to be equipped with large-scale antenna arrays [5], which leads to high hardware cost (HWC).

One mature technological solution to these problems is the multi-hop transmission scheme called relaying. Conventional wireless cooperative communication systems mostly employ relays [6]–[9] to process on the signals received halfway and retransmit the signals to the destination terminals actively through an uncontrollable propagation environment. Relays are validated to be effective on improving system reliability [7], but are still active retransmitting facilities that require high energy consumption (EC) and HWC. Recently, another state of the art approach, which is named Intelligent Reflecting Surface (IRS) [10], [11], Large Intelligent Surface (LIS) [2] or Large Intelligent Metasurface (LIM) [12], has attracted extensive attentions from wireless communication researchers. An IRS is a planar array composed of a large number of low-cost passive reconfigurable reflecting elements, each of which induces an adjustable phase shift on the coming signal wave and reflects the signal to the destination terminal [13]. It is distinguished from the ordinary physical reflecting surfaces which simply reflect the signal waves without any parameter adjustment, and also different from the traditional relays which actively retransmit the received signals. As a passive reflecting apparatus, the IRS is envisioned as a promising hardware solution to EC and HWC in the future communication networks.

There have already been studies that focused on the modulation schemes, secure communication realizations, phase shift optimizations, channel estimations and capacity analyses on the IRS-aided wireless communication systems [2], [14]–[18]. For instance, E. Basar [14] proposed an IRS-based index modulation scheme which enabled high data rates and low bit-error-rates (BER). M. Cui, *et al.* [15] and H. Shen, *et al.* [16] developed IRS-aided secure wireless communication systems where the IRS was employed to maximize the rate gap (secrecy rate) between the desired transmission path from the source to the legitimate user and the undesired one from the source to the eavesdropper. W. Yan, *et al.* [2] developed a passive beamforming and information

transferring method and optimized the phase shifts with different state values to improve the average signal-to-noise ratio (SNR). Q. Nadeem, *et al.* [17] outlined an IRS-aided multi-user MIMO communication system and estimated the cascaded channel matrix within each time interval. E. Bjrnson, *et al.* [18] analysed and compared the channel capacities of the IRS-supported, the decode-and-forward (DF) relay assisted and the single-input-single-output (SISO) systems, and derived the least required number of IRS reflecting elements which allowed the IRS to outperform DF relay and SISO.

The aforementioned works are carried out under the assumption of perfect IRS hardware. However, in most practical situations, inherent hardware impairments (HWI) such as phase noises, quantization errors, amplifier non-linearities, *et al.*, which generally limit the system performance, cannot be neglected due to the non-idealities of the communication devices in the real world [8], [19], [20]. Although the effect of the HWI on the system performance can be mitigated by compensation algorithms [21], there will still exist residual HWI due to imprecisely estimated time-variant hardware characteristics and random noises. As a result, it is of great significance to probe into the system performance in the presence of HWI. Some researchers [22]–[24] analysed the channel capacity of the massive MIMO systems with HWI, which they modelled as additive Gaussian distributed distortion noises. But to the best of our knowledge, there were only a few studies that analysed the IRS-aided systems with HWI of the IRS (I-HWI) [25], [26]. Among these studies, the researchers modelled I-HWI as additive variables in relation to the distances between reflecting points and the reflecting surface center [25], or as uniformly distributed phase noises generated by reflecting units [26]. However, investigations in these works might not be thorough enough as they did not take the HWI of the transmitting devices and receiving terminals into consideration, which would jointly influence the performance of the IRS-aided communication systems as well. Up to now, we have not found relative works that analysed the performance of the IRS-aided systems with the consideration of the HWI of both IRS and transceivers (IT-HWI) yet. Therefore, in this article we provide achievable rate (ACR) analyses and phase shift optimizations for the IRS-aided communication systems with I-HWI and IT-HWI, and present performance comparisons with the existing DF relay assisted systems with the HWI of the DF relay and transceivers. Our contributions are summarized as follows.

By referring to [26], we model I-HWI as uniformly distributed random phase errors generated by IRS reflecting units. When the IRS phase shifts are adjusted to compensate for the phase shifts in the wireless channels from the transmitting source to the IRS and from the IRS to the receiving destination, we analyse the ACR and mathematically derive the closed-form expression of the average ACR in relation to the number of reflecting elements (N) with I-HWI. As the transceiver HWI should not be ignored under actual circumstances, we also analyse the ACR with IT-HWI and obtain the closed-form expression in relation

to N . From the theoretical and numerical results, we confirm that the average ACR with HWI is lower than that without HWI, and both of them increase as N grows.

In order to optimize the IRS phase shifts and obtain the maximum average ACR with I-HWI or IT-HWI, we formulate the optimization problems and transform the non-convex problems into convex semidefinite programming (SDP) problems. By exploiting CVX toolbox in the MATLAB simulations, we derive the optimization results numerically, from which we conclude that the maximum average ACR with HWI is lower than that without HWI, and both of them increase as N grows.

We theoretically compare the average ACR of the IRS-aided communication system with that of the DF relay assisted communication system when there exist the HWI of the IRS, DF relay and transceivers. Specifically, we derive the least number of N which is required for the IRS to outperform single-antenna DF relay, and obtain the conditions where the IRS can always surpass single-antenna DF relay for all N . We also numerically compare the performance of the IRS with that of the multi-antenna DF relay equipped with N antennas. From the comparisons, we conclude that when N is large enough, the IRS can outperform DF relay in the presence of HWI.

The rest of this article is organized as follows. In Section II, we introduce the IRS-aided communication system model with HWI. In Section III, we analyse the ACRs of the IRS-aided communication systems with I-HWI and IT-HWI. In Section IV, we formulate the optimization problems to optimize the IRS phase shifts with I-HWI and IT-HWI. In Section V, we mathematically compare the average ACR with that of the DF relay assisted communication system in the presence of the HWI of the IRS, DF relay and transceivers. In Section VI, we provide numerical results to verify the theoretical analyses. In Section VII, we draw the overall conclusions.

Notations: Italics denote the variables or constants, while boldfaces denote the vectors or matrices. \mathbf{A}^* , \mathbf{A}^T , \mathbf{A}^H and \mathbf{A}^{-1} symbolize the conjugate, transpose, conjugate-transpose and inverse of matrix \mathbf{A} , respectively. $\text{tr}(\mathbf{A})$ and $\text{rank}(\mathbf{A})$ stand for the trace and the rank of \mathbf{A} . $\text{diag}(\mathbf{a})$ represents an $n \times n$ sized diagonal matrix whose diagonal elements are (a_1, a_2, \dots, a_n) in vector \mathbf{a} . $\|\cdot\|_2$ represents ℓ_2 norm. $\mathbf{A} \in \mathbb{C}^{m \times n}$ or $\mathbf{A} \in \mathbb{R}^{m \times n}$ means that \mathbf{A} is an $m \times n$ sized complex or real-numbered matrix. $\mathbf{A} \sim \mathcal{CN}(\mathbf{0}, \mathbf{V})$ illustrates that \mathbf{A} obeys complex normal distribution with mean of zero and covariance matrix of \mathbf{V} . $\mathbf{A} \succeq \mathbf{0}$ means that \mathbf{A} is positive semidefinite. $\mathbb{E}_{\mathbf{x}}[\mathbf{A}]$ denotes the expectation of \mathbf{A} on the random variable \mathbf{x} if \mathbf{A} is a stochastic matrix in relation to \mathbf{x} . \mathbf{I}_n and $\mathbf{\Gamma}_n$ symbolize $n \times n$ sized identity matrix and $n \times n$ sized matrix with all elements of 1, respectively. $\mathbf{1}$ stands for the unit row vector with all elements of 1. $\Delta = b^2 - 4ac$ represents the discriminant of the quadratic function $f(x) = ax^2 + bx + c$.

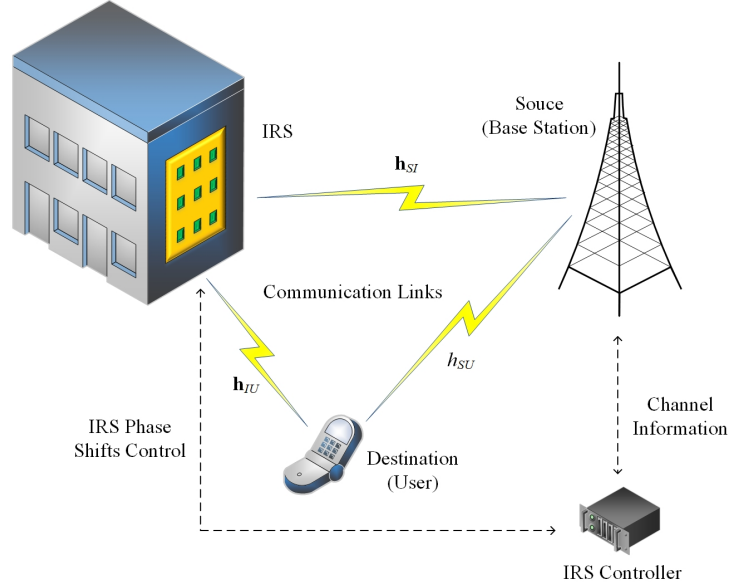


Fig. 1: The considered IRS-aided wireless communication system, which includes a single-antenna source, a single-antenna destination, an IRS with N reflecting elements and an IRS controller. The IRS controller is applied to adjust the IRS phase shifts based on the channel information.

II. COMMUNICATION SYSTEM MODEL

In this article, the considered wireless communication system (Figure 1) includes a signal-emitting source (e.g. the base station), an IRS with N reflecting elements and a signal-receiving destination (e.g. the user). The signal-emitting source, assumed to be equipped with single antenna, transmits the modulated signals with an average signal power of \sqrt{P} . The IRS induces adjustable phase shifts on the impinging signals and reflects the coming signal waves to the destination. The signal-receiving destination, also equipped with single antenna, receives the directly arrived signals from the source and passively reflected signals from the IRS.

Generally, due to the non-ideality of the hardware, the received signal is disturbed by the HWI which universally exists in the real-world communication devices. In this considered system, there are two kinds of HWI including I-HWI and transceiver HWI with different mathematical models. First, the I-HWI is modelled as a random diagonal phase error matrix, which contains N random phase errors induced by intrinsic hardware non-idealities of the reflectors, or by imprecisions of channel estimations [26]. It is expressed as $\mathbf{\Theta}_E = \text{diag}(e^{j\theta_{E1}}, e^{j\theta_{E2}}, \dots, e^{j\theta_{EN}})$, where θ_{Ei} , for $i = 1, 2, \dots, N$, are random phase errors uniformly distributed on $[-\pi/2, \pi/2]$. Thus, the received signal disturbed by I-HWI is modelled as

$$y = (\mathbf{h}_{IU}^T \mathbf{\Phi} \mathbf{\Theta}_E \mathbf{h}_{SI} + h_{SU}) \sqrt{P} s + w \quad (1)$$

where s stands for the unit-power signal symbol with $\mathbb{E}[ss^*] = 1$; $w \sim \mathcal{CN}(0, \sigma_w^2)$ denotes the

additive white Gaussian noise (AWGN); $\Phi = \alpha \text{diag}(e^{j\theta_1}, e^{j\theta_2}, \dots, e^{j\theta_N})$ represents the phase shifting matrix of the IRS, where $\alpha \in (0, 1]$ is the fixed amplitude reflection coefficient and θ_i , for $i = 1, 2, \dots, N$, are the adjustable phase-shift variables of the IRS; $h_{SU} = \sqrt{\mu_{SU}}e^{j\varphi_{SU}}$ represents the channel coefficient from the source to the destination, where $\sqrt{\mu_{SU}}$ and φ_{SU} are the power attenuation coefficient and the phase shift of h_{SU} ; $\mathbf{h}_{IU} \in \mathbb{C}^{N \times 1}$ and $\mathbf{h}_{SI} \in \mathbb{C}^{N \times 1}$ are the channel coefficients from the IRS to the destination and from the source to the IRS, respectively, which are expressed as $\mathbf{h}_{IU} = \sqrt{\mu_{IU}}(e^{j\varphi_{IU,1}}, e^{j\varphi_{IU,2}}, \dots, e^{j\varphi_{IU,N}})^T$ and $\mathbf{h}_{SI} = \sqrt{\mu_{SI}}(e^{j\varphi_{SI,1}}, e^{j\varphi_{SI,2}}, \dots, e^{j\varphi_{SI,N}})^T$, where $\sqrt{\mu_{IU}}$ and $\sqrt{\mu_{SI}}$ are the power attenuation coefficients of \mathbf{h}_{IU} and \mathbf{h}_{SI} ; $\varphi_{IU,i}$ and $\varphi_{SI,i}$, for $i = 1, 2, \dots, N$, are the phase shifts of \mathbf{h}_{IU} and \mathbf{h}_{SI} .

Then, the transceiver HWI is modelled as the additive distortion noise, which creates a mismatch between the intended signal and the practically generated signal, or creates a distortion on the received signal during the reception processing [22]. The distortion noises generated by the transmitter and the receiver are expressed as $\eta_t \sim \mathcal{CN}(0, \Upsilon_t)$ and $\eta_r \sim \mathcal{CN}(0, V_r)$, respectively, where $\Upsilon_t = \kappa_t P \mathbb{E}[ss^*]$ and $V_r = \kappa_r P |\mathbf{h}_{IU}^T \Phi \Theta_E \mathbf{h}_{SI} + h_{SU}|^2 \mathbb{E}[ss^*]$, as the distortion noises are proportional to the signal power. κ_t and κ_r represent the proportionality coefficients which describe the severities of the HWI at the transmitter and the receiver, respectively. Therefore, referring to Eq. (2) in [22], the received signal disturbed by IT-HWI is modelled as

$$y = (\mathbf{h}_{IU}^T \Phi \Theta_E \mathbf{h}_{SI} + h_{SU}) (\sqrt{P}s + \eta_t) + \eta_r + w \quad (2)$$

For this communication system, we would first analyse the ACR in relation to the number of IRS reflecting elements (N) in the presence of I-HWI, and calculate the rate gap between the ACR with I-HWI and that without I-HWI. As the transceiver HWI is also unavoidable because of the insufficiency of the accurate modelling, the time-variant characteristics, *et al.* [22], we would then analyse the ACR in the presence of IT-HWI without loss of generality, and calculate the rate gap between the ACR with IT-HWI and that without IT-HWI.

III. ACR ANALYSES WITH HWI

A. ACR Analyses with I-HWI

Based on the signal model in (1), we would first analyse the ACR of the considered IRS-aided communication system in the presence of I-HWI. Here we assume that the phase information in the cascaded channel model [17], [27] is already estimated before Φ is adjusted, so that $(\varphi_{IU,i} + \varphi_{SI,i})$, for $i = 1, 2, \dots, N$, are known for the IRS phase shift controller (this can be realized via some existing channel estimation techniques [17], [27]). In (1), $\mathbf{h}_{IU}^T \Phi \Theta_E \mathbf{h}_{SI}$ is maximized if each phase shift of the IRS is adjusted into $\theta_i = -(\varphi_{IU,i} + \varphi_{SI,i})$, for $i =$

$1, 2, \dots, N$, to compensate for the phase shifts in \mathbf{h}_{IU} and \mathbf{h}_{SI} [18]. As a result, when $\theta_i = -(\varphi_{IU,i} + \varphi_{SI,i})$, the received signal disturbed by I-HWI is expressed as

$$y = (\alpha \mathbf{g}_{IU}^T \Theta_E \mathbf{g}_{SI} + h_{SU}) \sqrt{P} s + w \quad (3)$$

where $\mathbf{g}_{IU} = \sqrt{\mu_{IU}} \mathbf{1}^T$ and $\mathbf{g}_{SI} = \sqrt{\mu_{SI}} \mathbf{1}^T$. Then, the ACR with I-HWI is expressed as

$$R_{I-HWI}(N) = \log_2 \left(1 + \frac{P |\alpha \mathbf{g}_{IU}^T \Theta_E \mathbf{g}_{SI} + h_{SU}|^2}{\sigma_w^2} \right) \quad (4)$$

Based on (4), we obtain the following theoretical results.

Theorem 1. When $\theta_i = -(\varphi_{IU,i} + \varphi_{SI,i})$ and θ_{Ei} is uniformly distributed on $[-\pi/2, \pi/2]$, the average ACR in the presence of I-HWI is expressed as

$$\overline{R_{I-HWI}}(N) = \log_2 \left[1 + \frac{P (\alpha^2 N \mu_{IU} \mu_{SI} + \frac{4\alpha N}{\pi} \sqrt{\mu_{IU} \mu_{SI} \mu_{SU}} \cos(\varphi_{SU}) + \mu_{SU})}{\sigma_w^2} \right] \quad (5)$$

Proof. The proof is given in Appendix A. \square

Let $R(N)$ denote the ACR without I-HWI. For theoretically comparing $\overline{R_{I-HWI}}(N)$ with $R(N)$ and investigating the impact that Θ_E has on the ACR, we would further calculate the rate gap between $\overline{R_{I-HWI}}(N)$ and $R(N)$, which is defined by $\Delta R(N) = R(N) - \overline{R_{I-HWI}}(N)$ in the following **Lemma 1**.

Lemma 1. When $\theta_i = -(\varphi_{IU,i} + \varphi_{SI,i})$ and θ_{Ei} is uniformly distributed on $[-\pi/2, \pi/2]$, the rate gap $\Delta R(N)$ between the average ACR with I-HWI and that without HWI is expressed as

$$\Delta R(N) = \log_2 \left[1 + \frac{N(N-1) P \alpha^2 \mu_{IU} \mu_{SI} + \frac{(2\pi-4)\alpha P}{\pi} N \sqrt{\mu_{IU} \mu_{SI} \mu_{SU}} \cos(\varphi_{SU})}{\sigma_w^2 + P \alpha^2 N \mu_{IU} \mu_{SI} + \frac{4\alpha P}{\pi} N \sqrt{\mu_{IU} \mu_{SI} \mu_{SU}} \cos(\varphi_{SU}) + P \mu_{SU}} \right] \quad (6)$$

Proof. According to [18], $R(N)$ is expressed as

$$R(N) = \log_2 \left[1 + \frac{P (\alpha^2 N^2 \mu_{IU} \mu_{SI} + 2\alpha N \sqrt{\mu_{IU} \mu_{SI} \mu_{SU}} \cos(\varphi_{SU}) + \mu_{SU})}{\sigma_w^2} \right] \quad (7)$$

Therefore, we calculate $\Delta R(N) = R(N) - \overline{R_{I-HWI}}(N)$ and then prove **Lemma 1**. \square

Theorem 1 illustrates that the SNR in $\overline{R_{I-HWI}}(N)$ is proportional to N while that in $R(N)$ is proportional to N^2 , which indicates that $\overline{R_{I-HWI}}(N)$ has a lower increasing speed than $R(N)$ as N grows. **Lemma 1** illustrates that $\Delta R(N) > 0$ when $N > 0$, which leads to $R(N) > \overline{R_{I-HWI}}(N)$ and demonstrates that the I-HWI will reduce the ACR by $\Delta R(N)$.

This part merely analyses the ACR with I-HWI. However, as the residual transceiver HWI is usually unavoidable in most practical communication systems, it is important to evaluate the

ACR in the presence of IT-HWI without loss of generality.

B. ACR Analyses with IT-HWI

Based on the signal model in (2), we would then analyse the ACR of the considered system in the presence of IT-HWI. Let $\theta_i = -(\varphi_{IU,i} + \varphi_{SI,i})$, and we can expand (2) into

$$y = (\alpha \mathbf{g}_{IU}^T \mathbf{\Theta}_E \mathbf{g}_{SI} + h_{SU}) \sqrt{P} s + (\alpha \mathbf{g}_{IU}^T \mathbf{\Theta}_E \mathbf{g}_{SI} + h_{SU}) \eta_t + \eta_r + w \quad (8)$$

Then, the ACR with IT-HWI is written as

$$\begin{aligned} R_{IT-HWI}(N) &= \log_2 \left(1 + \frac{P |\alpha \mathbf{g}_{IU}^T \mathbf{\Theta}_E \mathbf{g}_{SI} + h_{SU}|^2}{\kappa_t P |\alpha \mathbf{g}_{IU}^T \mathbf{\Theta}_E \mathbf{g}_{SI} + h_{SU}|^2 + \kappa_r P |\alpha \mathbf{g}_{IU}^T \mathbf{\Theta}_E \mathbf{g}_{SI} + h_{SU}|^2 + \sigma_w^2} \right) \\ &= \log_2 \left(1 + \frac{1}{\kappa_t + \kappa_r + \frac{\sigma_w^2}{P |\alpha \mathbf{g}_{IU}^T \mathbf{\Theta}_E \mathbf{g}_{SI} + h_{SU}|^2}} \right) \end{aligned} \quad (9)$$

from which we obtain the following **Theorem 2** and **Lemma 2**.

Theorem 2. When $\theta_i = -(\varphi_{IU,i} + \varphi_{SI,i})$ and θ_{Ei} is uniformly distributed on $[-\pi/2, \pi/2]$, the average ACR with IT-HWI is expressed as

$$\overline{R_{IT-HWI}}(N) = \log_2 \left[1 + \frac{1}{\kappa_t + \kappa_r + \frac{\sigma_w^2}{P \left(\alpha^2 N \mu_{IU} \mu_{SI} + \frac{4\alpha N}{\pi} \sqrt{\mu_{IU} \mu_{SI} \mu_{SU}} \cos(\varphi_{SU}) + \mu_{SU} \right)}} \right] \quad (10)$$

Proof. Similar to the proof of **Theorem 1**, we calculate the expectation of $P |\alpha \mathbf{g}_{IU}^T \mathbf{\Theta}_E \mathbf{g}_{SI} + h_{SU}|^2$ and then prove **Theorem 2**. \square

Lemma 2. When $\theta_i = -(\varphi_{IU,i} + \varphi_{SI,i})$ and θ_{Ei} is uniformly distributed on $[-\pi/2, \pi/2]$, the rate gap $\Delta R(N)$ between the average ACR with IT-HWI and that without HWI is expressed as

$$\Delta R(N) = \log_2 \left[\frac{P(\kappa_t + \kappa_r)\beta + \sigma_w^2 + P^2 \lambda \beta \left(\frac{\kappa_t}{\sigma_w^2} + \frac{\kappa_r}{\sigma_w^2} \right) + P\lambda}{P(\kappa_t + \kappa_r + 1)\beta + \sigma_w^2} \right] \quad (11)$$

where $\lambda = \alpha^2 N^2 \mu_{IU} \mu_{SI} + 2\alpha N \sqrt{\mu_{IU} \mu_{SI} \mu_{SU}} \cos(\varphi_{SU}) + \mu_{SU}$ and $\beta = \alpha^2 N \mu_{IU} \mu_{SI} + \frac{4\alpha N}{\pi} \times \sqrt{\mu_{IU} \mu_{SI} \mu_{SU}} \cos(\varphi_{SU}) + \mu_{SU}$.

Proof. We prove **Lemma 2** by calculating the rate gap according to $\Delta R(N) = R(N) - \overline{R_{IT-HWI}}(N)$, where $R(N)$ is expressed as (7) and $\overline{R_{IT-HWI}}(N)$ is expressed as (10). \square

Theorem 2 demonstrates that $\overline{R_{IT-HWI}}(N)$ is smaller than $\overline{R_{I-HWI}}(N)$. **Lemma 2** illustrates that $\Delta R(N) > 0$ when $N > 0$, and $\Delta R(N)$ increases as N grows, because the numerator

inside $\log_2(\cdot)$ includes λ which is proportional to N^2 , while the denominator inside $\log_2(\cdot)$ only contains β which is proportional to N . Results in **Theorem 1**, **Lemma 1**, **Theorem 2** and **Lemma 2** are derived on the basis of $\theta_i = -(\varphi_{IU,i} + \varphi_{SI,i})$ which is configured to compensate for the phase shifts in \mathbf{h}_{IU} and \mathbf{h}_{SI} [18]. However, $\theta_i = -(\varphi_{IU,i} + \varphi_{SI,i})$ might not be the optimal θ_i in this considered wireless propagation environment, as it does not take the phase shift in h_{SU} into account. Thus, in Section IV, we would optimize the IRS phase shifts and reconfigure the phase shifting matrix to obtain the maximum ACR with HWI.

IV. PHASE SHIFT OPTIMIZATION

Instead of simply configuring the IRS phase shifts to be $\theta_i = -(\varphi_{IU,i} + \varphi_{SI,i})$ to evaluate the ACR, we would present the problem formulations and phase shift optimizations on the IRS with I-HWI or IT-HWI in this section.

A. Optimization in the Presence of I-HWI

We would first optimize the IRS phase shifts when there exists I-HWI. Here we retrospect (1), from which we obtain the ACR with I-HWI:

$$R_{\Phi, I-HWI}(N) = \log_2 \left(1 + \frac{P |\mathbf{h}_{IU}^T \Phi \Theta_E \mathbf{h}_{SI} + h_{SU}|^2}{\sigma_w^2} \right) \quad (12)$$

Let \mathbf{D}_{IU} denote a diagonal matrix expressed as $\mathbf{D}_{IU} = \text{diag}(\mathbf{h}_{IU})$, and $\boldsymbol{\theta}$ denote a column vector expressed as $\boldsymbol{\theta} = \alpha (e^{j\theta_1}, e^{j\theta_2}, \dots, e^{j\theta_N})^T$. Then, we have $\boldsymbol{\theta}^T \mathbf{D}_{IU} = \mathbf{h}_{IU}^T \Phi$. By replacing $\mathbf{h}_{IU}^T \Phi$ with $\boldsymbol{\theta}^T \mathbf{D}_{IU}$, we expand (12) and obtain

$$R_{\boldsymbol{\theta}, I-HWI}(N) = \log_2 \left[1 + \frac{P (Z + h_{SU}^* h_{SU})}{\sigma_w^2} \right] \quad (13)$$

where $Z = \mathbf{h}_{SI}^H \Theta_E^H \mathbf{D}_{IU}^H \boldsymbol{\theta}^* \boldsymbol{\theta}^T \mathbf{D}_{IU} \Theta_E \mathbf{h}_{SI} + \mathbf{h}_{SI}^H \Theta_E^H \mathbf{D}_{IU}^H \boldsymbol{\theta}^* h_{SU} + h_{SU}^* \boldsymbol{\theta}^T \mathbf{D}_{IU} \Theta_E \mathbf{h}_{SI}$.

Let \mathbf{a} be defined by $\mathbf{a} = (\boldsymbol{\theta}^T, 1)^H$. We can rewrite Z as $Z = \mathbf{a}^H \Xi \mathbf{a}$, where

$$\Xi = \begin{pmatrix} \mathbf{D}_{IU} \Theta_E \mathbf{h}_{SI} \mathbf{h}_{SI}^H \Theta_E^H \mathbf{D}_{IU}^H & h_{SU}^* \mathbf{D}_{IU} \Theta_E \mathbf{h}_{SI} \\ \mathbf{h}_{SI}^H \Theta_E^H \mathbf{D}_{IU}^H h_{SU} & 0 \end{pmatrix} \quad (14)$$

Therefore, $R_{\boldsymbol{\theta}, I-HWI}(N)$ can be simplified into

$$R_{\boldsymbol{\theta}, I-HWI}(N) = \log_2 \left[1 + \frac{P (\mathbf{a}^H \Xi \mathbf{a} + \|h_{SU}\|_2^2)}{\sigma_w^2} \right] = \log_2 \left\{ 1 + \frac{P [\text{tr}(\Xi \mathbf{X}) + \|h_{SU}\|_2^2]}{\sigma_w^2} \right\} \quad (15)$$

where

$$\mathbf{X} = \mathbf{a} \mathbf{a}^H = \begin{pmatrix} \boldsymbol{\theta}^* \boldsymbol{\theta}^T & \boldsymbol{\theta}^* \\ \boldsymbol{\theta}^T & 1 \end{pmatrix} \in \mathbb{C}^{(N+1) \times (N+1)} \quad (16)$$

Consequently, the optimization problem is formulated as

$$\max_{\mathbf{X} \succeq \mathbf{0}} \frac{P}{\sigma_w^2} [tr(\mathbf{\Xi}\mathbf{X}) + ||h_{SU}||_2^2] \quad (17a)$$

$$s.t. \ tr(\mathbf{E}_n\mathbf{X}) = \alpha^2, \ n = 1, 2, \dots, N \quad (17b)$$

$$tr(\mathbf{E}_{N+1}\mathbf{X}) = 1 \quad (17c)$$

$$rank(\mathbf{X}) = 1 \quad (17d)$$

where "s.t." is the abbreviation of "subject to", and the (i, j) th element in \mathbf{E}_n is expressed as

$$[\mathbf{E}_n]_{i,j} = \begin{cases} 1, & i = j = n \\ 0, & otherwise \end{cases} \quad (18)$$

Because $\mathbf{\Theta}_E$ in $\mathbf{\Xi}$ is a stochastic diagonal matrix that contains N random phase errors uniformly distributed on $[-\pi/2, \pi/2]$, we should calculate the expectation of $\mathbf{\Xi}$, denoted by $\mathbb{E}_{\mathbf{\Theta}_E}[\mathbf{\Xi}]$, in order to obtain a statistical average optimization result.

$\mathbb{E}_{\mathbf{\Theta}_E}[\mathbf{\Xi}]$ can be written as

$$\mathbb{E}_{\mathbf{\Theta}_E}[\mathbf{\Xi}] = \mathbb{E}_{\mathbf{v}_E}[\mathbf{\Xi}] = \begin{pmatrix} \mathbf{D}_{IU}\mathbf{D}_{SI}\mathbb{E}_{\mathbf{v}_E}[\mathbf{v}_E\mathbf{v}_E^H] & \mathbf{D}_{SI}^H\mathbf{D}_{IU}^H & h_{SU}^*\mathbf{D}_{IU}\mathbf{D}_{SI}\mathbb{E}_{\mathbf{v}_E}[\mathbf{v}_E] \\ \mathbb{E}_{\mathbf{v}_E}[\mathbf{v}_E^H] & \mathbf{D}_{SI}^H\mathbf{D}_{IU}^H h_{SU} & 0 \end{pmatrix} \quad (19)$$

where $\mathbf{D}_{SI} = diag(\mathbf{h}_{SI})$ and $\mathbf{v}_E = (e^{j\theta_{E1}}, e^{j\theta_{E2}}, \dots, e^{j\theta_{EN}})^T$. $\mathbb{E}_{\mathbf{v}_E}[\mathbf{v}_E\mathbf{v}_E^H]$ which is expressed as

$$\mathbb{E}_{\mathbf{v}_E}[\mathbf{v}_E\mathbf{v}_E^H] = \begin{pmatrix} 1 & \mathbb{E}_{\Delta\theta}[e^{j\theta_{E1}-j\theta_{E2}}] & \dots & \mathbb{E}_{\Delta\theta}[e^{j\theta_{E1}-j\theta_{EN}}] \\ \mathbb{E}_{\Delta\theta}[e^{j\theta_{E2}-j\theta_{E1}}] & 1 & \dots & \mathbb{E}_{\Delta\theta}[e^{j\theta_{E2}-j\theta_{EN}}] \\ \vdots & \vdots & \ddots & \vdots \\ \mathbb{E}_{\Delta\theta}[e^{j\theta_{EN}-j\theta_{E1}}] & \mathbb{E}_{\Delta\theta}[e^{j\theta_{EN}-j\theta_{E2}}] & \dots & 1 \end{pmatrix} \quad (20)$$

represents the autocorrelation matrix of \mathbf{v}_E , where $\Delta\theta = \theta_{Ei} - \theta_{Ej}$ obeys triangular distribution on $[-\pi, \pi]$ as θ_{Ei} obeys uniform distribution on $[-\pi/2, \pi/2]$ (detailed in Appendix A). Because $\mathbb{E}_{\Delta\theta}[e^{j\theta_{Ei}-j\theta_{Ej}}] = \mathbb{E}_{\Delta\theta}[e^{j\Delta\theta}] = \int_{-\pi}^{\pi} f(\Delta\theta) e^{j\Delta\theta} d\Delta\theta = 0$, where $f(\Delta\theta)$, expressed as (47) in Appendix A, is the probability density function of $\Delta\theta$, we have $\mathbb{E}_{\mathbf{v}_E}[\mathbf{v}_E\mathbf{v}_E^H] = \mathbf{I}_N$.

Moreover, because $\mathbb{E}_{\mathbf{v}_E}[\mathbf{v}_E] = (\mathbb{E}_{\theta_{E1}}[e^{j\theta_{E1}}], \mathbb{E}_{\theta_{E2}}[e^{j\theta_{E2}}], \dots, \mathbb{E}_{\theta_{EN}}[e^{j\theta_{EN}}])^T$ and $\mathbb{E}_{\theta_{Ei}}[e^{j\theta_{Ei}}] = \int_{-\pi/2}^{\pi/2} f(\theta_{Ei}) e^{j\theta_{Ei}} d\theta_{Ei} = \int_{-\pi/2}^{\pi/2} f(\theta_{Ei}) (\cos\theta_{Ei} + j\sin\theta_{Ei}) d\theta_{Ei} = 2/\pi$ for $i = 1, 2, \dots, N$, where $f(\theta_{Ei}) = 1/\pi$ is the probability density function of θ_{Ei} , we have $\mathbb{E}_{\mathbf{v}_E}[\mathbf{v}_E] = (2/\pi) \mathbf{1}^T$.

By substituting $\mathbb{E}_{\mathbf{v}_E}[\mathbf{v}_E\mathbf{v}_E^H] = \mathbf{I}_N$ and $\mathbb{E}_{\mathbf{v}_E}[\mathbf{v}_E] = (2/\pi) \mathbf{1}^T$ into (19), we have

$$\mathbb{E}_{\mathbf{\Theta}_E}[\mathbf{\Xi}] = \begin{pmatrix} \mathbf{D}_{IU}\mathbf{D}_{SI}\mathbf{I}_N\mathbf{D}_{SI}^H\mathbf{D}_{IU}^H & \frac{2}{\pi} h_{SU}^*\mathbf{D}_{IU}\mathbf{D}_{SI}\mathbf{1}^T \\ \frac{2}{\pi} \mathbf{1}\mathbf{D}_{SI}^H\mathbf{D}_{IU}^H h_{SU} & 0 \end{pmatrix} \quad (21)$$

Consequently, by replacing Ξ in (15) with $\mathbb{E}_{\Theta_E} [\Xi]$, we obtain the statistical average ACR:

$$\overline{R_{\theta, I-HWI}}(N) = \log_2 \left\{ 1 + \frac{P [tr(\mathbb{E}_{\Theta_E} [\Xi] \mathbf{X}) + ||h_{SU}||_2^2]}{\sigma_w^2} \right\} \quad (22)$$

and formulate the optimization problem as

$$\max_{\mathbf{X} \succeq \mathbf{0}} \frac{P}{\sigma_w^2} [tr(\mathbb{E}_{\Theta_E} [\Xi] \mathbf{X}) + ||h_{SU}||_2^2] \quad (23a)$$

$$s.t. \ tr(\mathbf{E}_n \mathbf{X}) = \alpha^2, \ n = 1, 2, \dots, N \quad (23b)$$

$$tr(\mathbf{E}_{N+1} \mathbf{X}) = 1 \quad (23c)$$

$$rank(\mathbf{X}) = 1 \quad (23d)$$

Problem (23) can be relaxed if the constraint of $rank(\mathbf{X}) = 1$ is removed. Thus, the relaxed problem is formulated as

$$\max_{\mathbf{X} \succeq \mathbf{0}} \frac{P}{\sigma_w^2} [tr(\mathbb{E}_{\Theta_E} [\Xi] \mathbf{X}) + ||h_{SU}||_2^2] \quad (24a)$$

$$s.t. \ tr(\mathbf{E}_n \mathbf{X}) = \alpha^2, \ n = 1, 2, \dots, N \quad (24b)$$

$$tr(\mathbf{E}_{N+1} \mathbf{X}) = 1 \quad (24c)$$

which is a SDP problem and can be solved by existing techniques [28]. It is remarkable that after Problem (24) is solved, the θ^T in the $(N+1)th$ row of the \mathbf{X} in the solution can be extracted to reconstruct \mathbf{X} based on (16). The reconstructed \mathbf{X} , denoted by \mathbf{X}_r , is numerically testified to be $\mathbf{X}_r = \mathbf{X}$ where the \mathbf{X} is derived from the solution, and the rank of \mathbf{X}_r is testified to be $rank(\mathbf{X}_r) = 1$ even if the original problem is relaxed (detailed in Appendix B). As a result, we can obtain the optimal IRS phase shifts from θ^T in the $(N+1)th$ row of the \mathbf{X} in the solution of the relaxed problem.

B. Optimization in the Presence of IT-HWI

We would then optimize the IRS phase shifts in the presence of IT-HWI. We retrospect (2) from which we obtain the ACR with IT-HWI:

$$\begin{aligned} R_{\Phi, IT-HWI}(N) &= \log_2 \left(1 + \frac{P |\mathbf{h}_{IU}^T \Phi \Theta_E \mathbf{h}_{SI} + h_{SU}|^2}{\kappa_t P |\mathbf{h}_{IU}^T \Phi \Theta_E \mathbf{h}_{SI} + h_{SU}|^2 + \kappa_r P |\mathbf{h}_{IU}^T \Phi \Theta_E \mathbf{h}_{SI} + h_{SU}|^2 + \sigma_w^2} \right) \\ &= \log_2 \left\{ 1 + \frac{P [tr(\Xi \mathbf{X}) + ||h_{SU}||_2^2]}{P (\kappa_t + \kappa_r) [tr(\Xi \mathbf{X}) + ||h_{SU}||_2^2] + \sigma_w^2} \right\} \end{aligned} \quad (25)$$

Therefore, the optimization problem is formulated as

$$\max_{\mathbf{X} \succeq \mathbf{0}} \frac{P [\text{tr}(\mathbf{\Xi}\mathbf{X}) + ||h_{SU}||_2^2]}{P(\kappa_t + \kappa_r) [\text{tr}(\mathbf{\Xi}\mathbf{X}) + ||h_{SU}||_2^2] + \sigma_w^2} \quad (26a)$$

$$s.t. \text{tr}(\mathbf{E}_n\mathbf{X}) = \alpha^2, \quad n = 1, 2, \dots, N \quad (26b)$$

$$\text{tr}(\mathbf{E}_{N+1}\mathbf{X}) = 1 \quad (26c)$$

Problem (26) is a non-convex problem. Hence, let \mathbf{Y} and μ be defined by $\mathbf{Y} = \mu\mathbf{X}$ and $\mu = \frac{1}{\text{tr}(\mathbf{\Xi}\mathbf{X}) + ||h_{SU}||_2^2 + \frac{\sigma_w^2}{P(\kappa_t + \kappa_r)}}$. Then, the objective function in (26) is expressed as $\frac{1}{(\kappa_t + \kappa_r)} \times [\text{tr}(\mathbf{\Xi}\mathbf{Y}) + \mu||h_{SU}||_2^2]$. Therefore, Problem (26) can be transformed into

$$\max_{\mathbf{Y} \succeq \mathbf{0}} \frac{1}{(\kappa_t + \kappa_r)} \times [\text{tr}(\mathbf{\Xi}\mathbf{Y}) + \mu||h_{SU}||_2^2] \quad (27a)$$

$$s.t. \text{tr}(\mathbf{E}_n\mathbf{Y}) = \mu\alpha^2, \quad n = 1, 2, \dots, N \quad (27b)$$

$$\text{tr}(\mathbf{E}_{N+1}\mathbf{Y}) = \mu \quad (27c)$$

$$\text{tr}(\mathbf{\Xi}\mathbf{Y}) + \mu \left[||h_{SU}||_2^2 + \frac{\sigma_w^2}{P(\kappa_t + \kappa_r)} \right] = 1 \quad (27d)$$

Similarly, in order to obtain the maximum average ACR in the presence of IT-HWI, by replacing $\mathbf{\Xi}$ with $\mathbb{E}_{\Theta_E}[\mathbf{\Xi}]$, we can formulate the optimization problem as

$$\max_{\mathbf{Y} \succeq \mathbf{0}} \frac{1}{(\kappa_t + \kappa_r)} \times [\text{tr}(\mathbb{E}_{\Theta_E}[\mathbf{\Xi}]\mathbf{Y}) + \mu||h_{SU}||_2^2] \quad (28a)$$

$$s.t. \text{tr}(\mathbf{E}_n\mathbf{Y}) = \mu\alpha^2, \quad n = 1, 2, \dots, N \quad (28b)$$

$$\text{tr}(\mathbf{E}_{N+1}\mathbf{Y}) = \mu \quad (28c)$$

$$\text{tr}(\mathbb{E}_{\Theta_E}[\mathbf{\Xi}]\mathbf{Y}) + \mu \left[||h_{SU}||_2^2 + \frac{\sigma_w^2}{P(\kappa_t + \kappa_r)} \right] = 1 \quad (28d)$$

where $\mu = \frac{1}{\text{tr}(\mathbb{E}_{\Theta_E}[\mathbf{\Xi}]\mathbf{X}) + ||h_{SU}||_2^2 + \frac{\sigma_w^2}{P(\kappa_t + \kappa_r)}}$. Problem (27) and (28) are currently SDP problems and can be solved by existing techniques [28].

V. ACR COMPARISONS WITH DF RELAY

The DF relay is a conventional active device which is also applied for data transmission enhancement in the wireless communication network. Hence, it is important to compare the performance of the IRS with that of the DF relay in the same situation. It was already confirmed that the ideal-hardware IRS equipped with a large number of reflecting units (N) could help the wireless communication system provide higher ACR than the ideal-hardware single-antenna DF relay [18]. In this section, for the purpose of exploring whether the IRS-aided system can still possess advantages in ACR over the single-antenna DF relay assisted system when there exists

HWI, we would theoretically compare the ACR of these two systems in the presence of IT-HWI and investigate which one would perform better under two different conditions.

Let h_{SR} , h_{RU} and h_{SU} denote the channel coefficients from the source to the DF relay, from the DF relay to the destination and from the source to the destination, respectively. The DF relay is assumed to be equipped with single antenna so that h_{SR} , h_{RU} and h_{SU} are complex values, which are expressed as $h_{SR} = \sqrt{\mu_{SR}}e^{j\varphi_{SR}}$, $h_{RU} = \sqrt{\mu_{RU}}e^{j\varphi_{RU}}$ and $h_{SU} = \sqrt{\mu_{SU}}e^{j\varphi_{SU}}$, where $\sqrt{\mu_{SR}}$, $\sqrt{\mu_{RU}}$ and $\sqrt{\mu_{SU}}$ represent the power attenuation factors; φ_{SR} , φ_{RU} and φ_{SU} represent the phase shifts in h_{SR} , h_{RU} and h_{SU} . For making comparisons, we assume that $\sqrt{\mu_{SR}} = \sqrt{\mu_{SI}}$, $\sqrt{\mu_{RU}} = \sqrt{\mu_{IU}}$, and the AWGN at the DF relay (w_{DF}) and the destination terminal (w) have the same variance of σ_w^2 . If there exists HWI in the source transmitter, DF relay and destination receiver, the signals received by the DF relay and the destination terminal are expressed as

$$y_{DF} = h_{SR} \left(\sqrt{P_1} s + \eta_t \right) + \eta_{r_{DF}} + w_{DF} = h_{SR} \sqrt{P_1} s + h_{SR} \eta_t + \eta_{r_{DF}} + w_{DF} \quad (29)$$

and

$$y_{U1} = h_{RU} \left(\sqrt{P_2} s + \eta_{t_{DF}} \right) + \eta_{r1} + w = h_{RU} \sqrt{P_2} s + h_{RU} \eta_{t_{DF}} + \eta_{r1} + w \quad (30)$$

$$y_{U2} = h_{SU} \left(\sqrt{P_1} s + \eta_t \right) + \eta_{r2} + w = h_{SU} \sqrt{P_1} s + h_{SU} \eta_t + \eta_{r2} + w \quad (31)$$

where P_1 and P_2 are the transmitting powers of the source and the DF relay under the constraint of $P = (P_1 + P_2)/2$ [18]; y_{U1} and y_{U2} are the signals received by the destination terminal through channel h_{RU} and h_{SU} , respectively; $\eta_t \sim \mathcal{CN}(0, \Upsilon_t)$, $\eta_{r_{DF}} \sim \mathcal{CN}(0, V_{r_{DF}})$, $\eta_{t_{DF}} \sim \mathcal{CN}(0, \Upsilon_{t_{DF}})$, $\eta_{r1} \sim \mathcal{CN}(0, V_{r1})$ and $\eta_{r2} \sim \mathcal{CN}(0, V_{r2})$ represent the additive distortion noises generated by the source transmitter, DF-relay receiver, DF-relay transmitter and destination receiver, where $\Upsilon_t = \kappa_t P_1 \mathbb{E}[ss^*]$, $V_{r_{DF}} = \kappa_{r_{DF}} P_1 |h_{SR}|^2 \mathbb{E}[ss^*]$, $\Upsilon_{t_{DF}} = \kappa_{t_{DF}} P_2 \mathbb{E}[ss^*]$, $V_{r1} = \kappa_{r1} P_2 |h_{RU}|^2 \mathbb{E}[ss^*]$ and $V_{r2} = \kappa_{r2} P_1 |h_{SU}|^2 \mathbb{E}[ss^*]$; κ_t , $\kappa_{r_{DF}}$, $\kappa_{t_{DF}}$, κ_{r1} and κ_{r2} are the proportionality factors.

For simple analyses, we consider that $\kappa_{t_{DF}} = \kappa_t$ and $\kappa_{r1} = \kappa_{r2} = \kappa_{r_{DF}} = \kappa_r$, as the hardware characteristics of the transceivers in the DF relay are similar to those in the source equipment and destination terminal. Therefore, referring to Eq. (15) in [29], the ACR of the DF relay assisted system with HWI of the relay and transceivers is expressed as

$$R_{DF,HWI} = \frac{1}{2} \min \{ \mathfrak{A}, \mathfrak{B} \} \quad (32)$$

where

$$\mathfrak{A} = \log_2 \left(1 + \frac{P_1 \mu_{SI}}{\kappa_t P_1 \mu_{SI} + \kappa_r P_1 \mu_{SI} + \sigma_w^2} \right) = \log_2 \left(1 + \frac{1}{\kappa_t + \kappa_r + \frac{\sigma_w^2}{P_1 \mu_{SI}}} \right) \quad (33)$$

$$\begin{aligned}
\mathfrak{B} &= \log_2 \left(1 + \frac{P_1 \mu_{SU}}{\kappa_t P_1 \mu_{SU} + \kappa_r P_1 \mu_{SU} + \sigma_w^2} + \frac{P_2 \mu_{IU}}{\kappa_t P_2 \mu_{IU} + \kappa_r P_2 \mu_{IU} + \sigma_w^2} \right) \\
&= \log_2 \left(1 + \frac{1}{\kappa_t + \kappa_r + \frac{\sigma_w^2}{P_1 \mu_{SU}}} + \frac{1}{\kappa_t + \kappa_r + \frac{\sigma_w^2}{P_2 \mu_{IU}}} \right)
\end{aligned} \tag{34}$$

It is remarkable that the expression of $R_{DF,HWI}$ in (32) is determined by \mathfrak{A} and \mathfrak{B} . Specifically, $R_{DF,HWI} = \frac{1}{2}\mathfrak{A}$ if $\mathfrak{A} < \mathfrak{B}$ and $R_{DF,HWI} = \frac{1}{2}\mathfrak{B}$ if $\mathfrak{A} > \mathfrak{B}$. Therefore, we would present our discussions under the following two conditions.

A. Condition 1: $\mathfrak{A} < \mathfrak{B}$

The condition of $\mathfrak{A} < \mathfrak{B}$ is detailed in the following **Lemma 3**.

Lemma 3. *For holding $\mathfrak{A} < \mathfrak{B}$, the transmitting powers and the channel attenuation coefficients should satisfy the following relationships:*

$$\frac{P_2}{P_1} > \frac{\mu_{SI}}{\mu_{IU}} \quad \text{and} \quad \mu_{SU} < \mu_{SI} \tag{35}$$

or

$$\frac{P_2}{P_1} < \frac{\mu_{SI}}{\mu_{IU}} \quad \text{and} \quad \mu_{SU} > \mu_{SI} \tag{36}$$

Proof. The proof is given in Appendix C. \square

Lemma 3 illustrates that if the total transmitting power of the DF relay assisted system ($P_1 + P_2 = 2P$) is allocated by $P_1 = P_2 = P$, the channel attenuation coefficients should satisfy $\mu_{SU} < \mu_{SI} < \mu_{IU}$ to meet (35) or satisfy $\mu_{SU} > \mu_{SI} > \mu_{IU}$ to meet (36). In most practical situations, μ_{SU} is the smallest among these three coefficients, as the distance between the source and the destination is usually longer than the distance between the source and the DF relay or the DF relay and the destination. Thus, we consider (35) in subsequent comparisons and discussions.

B. Condition 2: $\mathfrak{A} > \mathfrak{B}$

The condition of $\mathfrak{A} > \mathfrak{B}$ is detailed in the following **Lemma 4**.

Lemma 4. *For holding $\mathfrak{A} > \mathfrak{B}$, the transmitting powers, channel attenuation coefficients, and proportionality factors of the distortion noises should satisfy the following relationships:*

$$\frac{P_2}{P_1} > \frac{\mu_{SI}}{\mu_{IU}} \quad \text{and} \quad \mu_{SU} > \mu_{SI} \tag{37}$$

or

$$\frac{P_2}{P_1} < \frac{\mu_{SI}}{\mu_{IU}} \quad \text{and} \quad \mu_{SU} < \mu_{SI} \tag{38}$$

$\kappa_t + \kappa_r$ should satisfy:

$$\kappa_t + \kappa_r < \frac{\sigma_w^2}{P_1 \mu_{SI}} \left(\sqrt{\frac{(\mu_{IU} P_2 - \mu_{SI} P_1) (\mu_{SU} - \mu_{SI})}{P_2 \mu_{IU} \mu_{SU}}} - 1 \right) \quad (39)$$

Proof. The proof is given in Appendix D. \square

It is demonstrated in **Lemma 4** that if the total transmitting power of the DF relay assisted system is allocated by $P_1 = P_2 = P$, the channel attenuation coefficients should satisfy $\mu_{IU} > \mu_{SU} > \mu_{SI}$ in order to meet (37) or satisfy $\mu_{SU} < \mu_{IU} < \mu_{SI}$ in order to meet (38). For the same reason, we consider (38) in subsequent comparisons and discussions. Meanwhile, $\kappa_t + \kappa_r$ should satisfy (39), otherwise the result will turn into *Condition 1*.

C. Comparisons and Discussions

Based on the above analyses, we have $R_{DF,HWI} = \frac{1}{2}\mathfrak{A}$ under *Condition 1* and $R_{DF,HWI} = \frac{1}{2}\mathfrak{B}$ under *Condition 2*. Subsequently, we compare $\overline{R_{IT-HWI}}(N)$ in (10) with $R_{DF,HWI}$ and obtain the following theoretical results:

Theorem 3. *When the IRS outperforms DF relay, the number of IRS reflecting elements (N) should satisfy*

$$N > \frac{\frac{\sigma_w^2(\xi-1)}{P[1-(\xi-1)(\kappa_t+\kappa_r)]} - \mu_{SU}}{\alpha^2 \mu_{IU} \mu_{SI} + \frac{4\alpha}{\pi} \sqrt{\mu_{IU} \mu_{SI} \mu_{SU}} \cos(\varphi_{SU})} \quad (40)$$

where ξ is expressed as $\xi = \xi_{C1} = \sqrt{1 + \frac{1}{\kappa_t + \kappa_r + \frac{\sigma_w^2}{P_1 \mu_{SI}}}}$ under *Condition 1*, or expressed as $\xi = \xi_{C2} = \sqrt{1 + \frac{1}{\kappa_t + \kappa_r + \frac{\sigma_w^2}{P_1 \mu_{SU}}} + \frac{1}{\kappa_t + \kappa_r + \frac{\sigma_w^2}{P_2 \mu_{IU}}}}$ under *Condition 2*.

Proof. We prove this theorem by solving the range of N from $\overline{R_{IT-HWI}}(N) > R_{DF,HWI}$, which represents that the IRS performs better than DF relay on the average ACR. \square

For simple analyses, we assume that $\varphi_{SU} \in (-\pi/2, \pi/2)$ which results in $\cos(\varphi_{SU}) > 0$ as well as $\alpha^2 \mu_{IU} \mu_{SI} + \frac{4\alpha}{\pi} \sqrt{\mu_{IU} \mu_{SI} \mu_{SU}} \cos(\varphi_{SU}) > 0$. Then, **Theorem 3** demonstrates that the range of N is determined by $\frac{\sigma_w^2(\xi-1)}{P[1-(\xi-1)(\kappa_t+\kappa_r)]} - \mu_{SU}$, which is further determined by $\kappa_t + \kappa_r$ in a certain wireless propagation environment. If $\frac{\sigma_w^2(\xi-1)}{P[1-(\xi-1)(\kappa_t+\kappa_r)]} - \mu_{SU} < 0$, the IRS will always perform better than DF relay because N is identically larger than zero. Otherwise, the IRS will perform better than DF relay only when N satisfies (40). Because different $\kappa_t + \kappa_r$ causes different $\frac{\sigma_w^2(\xi-1)}{P[1-(\xi-1)(\kappa_t+\kappa_r)]} - \mu_{SU}$, we should theoretically compare the average ACR according to different $\kappa_t + \kappa_r$. The comparison results are detailed in the following **Lemma 5**.

Lemma 5. *Under Condition 1: when $P_1 = P_2 = P$, the IRS will always outperform DF relay for all $N > 0$ when $\kappa_t + \kappa_r$ satisfies*

$$\kappa_t + \kappa_r > \frac{2(S_{SI} - S_{SU})^2 - \left[S_{SU}^2 S_{SI} + S_{SU}(S_{SI} - S_{SU}) \sqrt{\left(\frac{S_{SU} S_{SI}}{S_{SI} - S_{SU}} \right)^2 + 4} \right]}{\left[S_{SU}^2 S_{SI}^2 + S_{SU} S_{SI}(S_{SI} - S_{SU}) \sqrt{\left(\frac{S_{SU} S_{SI}}{S_{SI} - S_{SU}} \right)^2 + 4} \right]} = \kappa_{th} \quad (41)$$

where $S_{SI} = \frac{P\mu_{SI}}{\sigma_w^2}$ and $S_{SU} = \frac{P\mu_{SU}}{\sigma_w^2}$. When $P_1 = P_2 = P$ and $\kappa_t + \kappa_r$ does not satisfy (41), the IRS performs better than DF relay when N satisfies (40) with $\xi = \xi_{C1}$.

Under Condition 2: when $P_1 = P_2 = P$, the IRS will always outperform DF relay for all $N > 0$ when $\kappa_t + \kappa_r$ simultaneously satisfies (39) and

$$\begin{cases} \kappa_t + \kappa_r > \frac{S_{IU} - S_{SU}^2 - S_{SU}}{S_{SU}^2 S_{IU} + S_{SU}^2 - S_{SU} S_{IU}} = \kappa_{th1}, & 1 + \frac{1}{S_{IU}} - \frac{1}{S_{SU}} > 0 \\ \kappa_t + \kappa_r < \frac{S_{IU} - S_{SU}^2 - S_{SU}}{S_{SU}^2 S_{IU} + S_{SU}^2 - S_{SU} S_{IU}} = \kappa_{th2}, & 1 + \frac{1}{S_{IU}} - \frac{1}{S_{SU}} < 0 \end{cases} \quad (42)$$

where $S_{IU} = \frac{P\mu_{IU}}{\sigma_w^2}$. When $P_1 = P_2 = P$ and $\kappa_t + \kappa_r$ satisfies (39) but does not satisfy (42), the IRS performs better than DF-relay when N satisfies (40) with $\xi = \xi_{C2}$.

Proof. The proof is given in Appendix E. □

From **Lemma 5** we can conclude that $\kappa_t + \kappa_r$ determines whether the IRS can always outperform DF relay for all $N > 0$, or can outperform DF relay only when N satisfies (40) by three demarcation values, which are κ_{th} in (41) under *Condition 1*, and κ_{th1} and κ_{th2} in (42) under *Condition 2*. κ_{th} is decided by S_{SI} and S_{SU} , which are further determined by μ_{SI} and μ_{SU} as they have the same P and σ_w^2 . Similarly, κ_{th1} and κ_{th2} are decided by S_{IU} and S_{SU} , which are further determined by μ_{IU} and μ_{SU} . μ_{SI} , μ_{IU} and μ_{SU} are generally relevant to the distances and path loss exponents between the source and the IRS, the IRS and the destination and the source and the destination, respectively [15]. Therefore, different system parameters will lead to different κ_{th} , κ_{th1} and κ_{th2} , and then lead to different comparison results, e.g. some system parameters will result in $\kappa_{th} < 0$, which will make the IRS always outperform DF relay no matter what $\kappa_t + \kappa_r$ and N are set under *Condition 1*; while the others will result in $\kappa_{th} \geq 0$, which will make the IRS conditionally outperform DF relay based on different $\kappa_t + \kappa_r$ and N . As a result, it is necessary to view the numerical comparisons with different $\kappa_t + \kappa_r$ and different κ_{th} , κ_{th1} and κ_{th2} . We would display these results in Section VI.

Besides, **Lemma 5** has also a physical interpretation, which illustrates that the IRS will possibly always surpass DF relay when the level of transceiver HWI is high enough. This is because the I-HWI is modelled as a phase error matrix which does not contain κ_t or κ_r , while the HWI of the DF relay is modelled as the distortion noise which contains the two terms. The

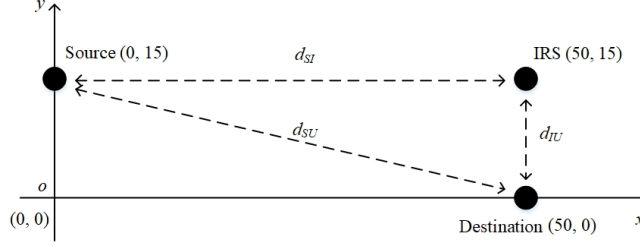


Fig. 2: Communication system design in the simulations. Distances and coordinates are measured in meters. Three dashed lines which indicate d_{SI} , d_{IU} and d_{SU} constitute a right triangle, where $d_{SU} = \sqrt{d_{SI}^2 + d_{IU}^2}$.

DF relay will perform worse with higher $\kappa_t + \kappa_r$ while the IRS will maintain the performance due to the fixed uniform distribution of the phase errors.

The above theoretical comparisons are made in consideration of single-antenna DF relay and multi-unit IRS. It is notable that as N grows, the average ACR of the IRS-aided system increases while that of the DF relay assisted system remains constant under a certain condition. This might be unfair for the DF relay during the comparisons. Therefore, it is important to compare the performance of the IRS with that of the multi-antenna DF relay which is also equipped with N antennas. However, as the channel coefficients include random phase shifts which cannot be compensated for by the DF relay, there does not exist a closed-form expression of the ACR in relation to N for the multi-antenna DF relay assisted system. Thus, we would provide these comparisons numerically in Section VI.

VI. NUMERICAL RESULTS

A. System Setup and Parameter Setting

This section would elaborate the numerical results of the ACR with or without HWI, and compare the ACR of the IRS-aided communication system with that of the DF relay assisted communication system. In this section, MATLAB 2019 is applied to conduct the simulations and to build the communication system described in Section II. A two-dimensional plane in meters is established to indicate the positions of the source, the IRS and the destination (Figure 2).

In Figure 2, the source, the IRS and the destination are placed at $(0, 15)$, $(50, 15)$ and $(50, 0)$. Regardless of the height, the distance between the source and the IRS (d_{SI}), the IRS and the destination (d_{IU}) and the source and the destination (d_{SU}) are $d_{SI} = 50$ m, $d_{IU} = 15$ m and $d_{SU} = \sqrt{d_{SI}^2 + d_{IU}^2} \approx 52.2$ m, respectively. The fixed amplitude reflection coefficient of the IRS is set to be $\alpha = 1$. According to [15], the other parameters are set as follows: The average signal power is set to be $\sqrt{P} = \sqrt{100}$ mW with $P = 20$ dBm. The noise power is set to be $\sigma_w^2 = -80$ dBm. The power attenuation coefficients of channel \mathbf{h}_{IU} (or h_{RU}), \mathbf{h}_{SI} (or h_{SR}) and h_{SU} are $\sqrt{\mu_{IU}} = \sqrt{\zeta_0(d_0/d_{IU})^{\alpha_{IU}}}$, $\sqrt{\mu_{SI}} = \sqrt{\zeta_0(d_0/d_{SI})^{\alpha_{SI}}}$ and $\sqrt{\mu_{SU}} = \sqrt{\zeta_0(d_0/d_{SU})^{\alpha_{SU}}}$,

where $\zeta_0 = -20$ dB denotes the path loss, $d_0 = 1$ m denotes the reference distance and $\alpha_{IU} = \alpha_{SI} = \alpha_{SU} = 3$ denote the path loss exponents. $\varphi_{IU,i}$ and $\varphi_{SI,i}$ are set to be random values within $[0, 2\pi]$. φ_{SU} is set to be $\varphi_{SU} = \pi/4$. The proportionality coefficients of the transceiver HWI are set to be $\kappa_t = \kappa_r = 0.05^2$.

During the comparisons with DF relay, d_{SI} , d_{IU} and d_{SU} are also regarded as the distances between the source and the DF relay, the DF relay and the destination, and the source and the destination, respectively, which are considered to be alterable but still adhere to $d_{SU} = \sqrt{d_{SI}^2 + d_{IU}^2}$. The path loss exponents and proportionality coefficients can be changed for diverse observations, but still satisfy $\alpha_{IU} = \alpha_{SI} = \alpha_{SU}$ and $\kappa_t = \kappa_r$.

B. ACR with I-HWI

For investigating the ACR with or without I-HWI, we carry out the simulations via the following steps:

Step 1: We calculate $\overline{R_{I-HWI}}(N)$ in (5) and record the results from $N = 10$ to $N = 100$.

Step 2: We calculate $R(N)$ in (7) and record the results from $N = 10$ to $N = 100$.

Step 3: We calculate and record the numerical results of $R_{I-HWI}(N)$ in (4) from $N = 10$ to $N = 100$. Due to the randomness of the phase errors generated by the IRS, the ACR is averaged on 1000 Monte Carlo trials at each N .

Step 4: We optimize the IRS phase shifts without HWI and record the ACR.

Step 5: We optimize the IRS phase shifts by solving Problem (24). Then, by substituting the optimized IRS phase shifts in θ^T in the $(N + 1)th$ row of \mathbf{X} into Φ in $R_{\Phi, I-HWI}(N)$ in (12), we obtain the ACR which is averaged on 1000 Monte Carlo trials at each N .

Step 6: We obtain the average ACR from the solution of Problem (24) at each N .

The average ACRs with or without I-HWI as functions of N from $N = 10$ to $N = 100$ are described in Figure 3. Results obtained from *Step 1* to *Step 6* are depicted by the lines with legends "With I-HWI (Theoretical)", "Without I-HWI", "With I-HWI (Experimental)", "Optimal without I-HWI", "Optimal with I-HWI (Experimental)" and "Optimal with I-HWI (Theoretical)", respectively. It is indicated in Figure 3 that: First, the overall experimental results fit well with the theoretical results from $N = 10$ to $N = 100$, which confirms that the theoretical relations in **Theorem 1** and (21) are correct. It is notable that the experimental results are higher than the theoretical results as N grows. This is because we calculate the expectation of the numerator of the SNR inside $\log_2\{\cdot\}$ instead of the ACR itself. Second, the average ACRs with $\theta_i = -(\varphi_{IU,i} + \varphi_{SI,i})$ are lower than those with optimized θ_i , which demonstrates that $\theta_i = -(\varphi_{IU,i} + \varphi_{SI,i})$ is not the optimal IRS phase shift. This phenomenon occurs because $\theta_i = -(\varphi_{IU,i} + \varphi_{SI,i})$ is only configured to compensate for the phase shifts in \mathbf{h}_{IU} and \mathbf{h}_{SI} , but does not take the phase shift in \mathbf{h}_{SU} into account. Third, the average ACRs with I-HWI

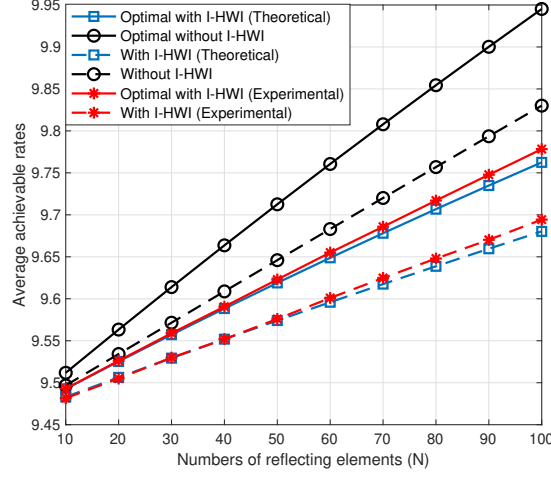


Fig. 3: Average ACRs as functions of N with or without I-HWI. The solid lines represent the ACRs with optimized IRS phase shifts, while the dashed lines represent the ACRs with $\theta_i = -(\varphi_{IU,i} + \varphi_{SI,i})$. The lines marked with * and Experimental stand for the experimental results, where each point represents an average result of 1000 Monte Carlo trials. The lines marked with \square and Theoretical stand for the statistical average results, specifically derived from (5) and Problem (24). The lines marked with \circ depict the results without I-HWI.

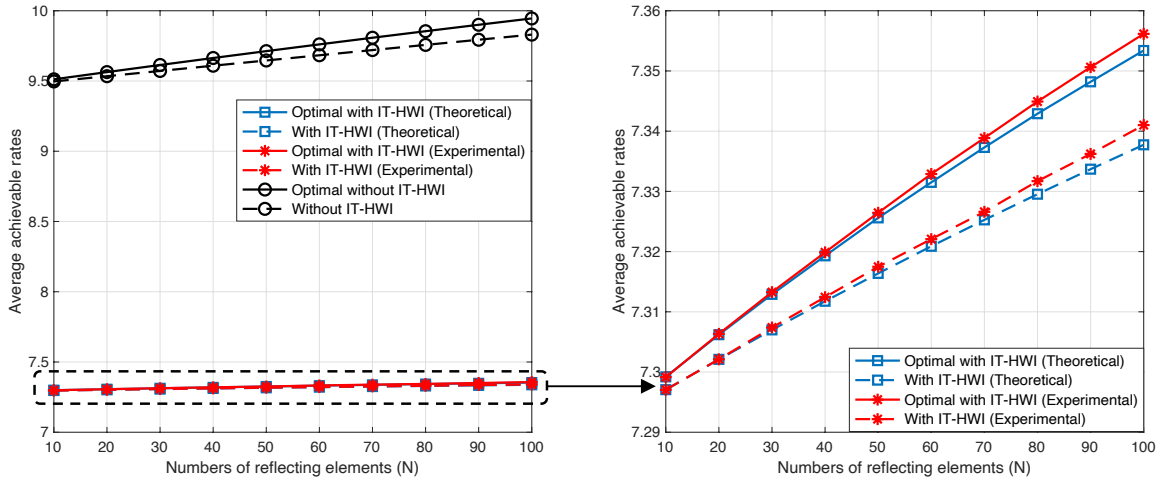


Fig. 4: Average ACRs as functions of N with or without IT-HWI. The descriptions are the same as those for Figure 3 except for: the lines marked with \square and Theoretical stand for the statistical average results, specifically derived from (10) and Problem (28); the lines marked with \circ depict the results without IT-HWI.

are lower and growing more slowly than those without I-HWI, and the rate gaps between the average ACRs with I-HWI and those without I-HWI widen as N grows.

C. ACR with IT-HWI

We would also display the ACR with or without IT-HWI numerically. We repeat *Step 1* to *Step 6* after we remain *Step 2* and *Step 4*, but replace *Step 1*, *Step 3*, *Step 5* and *Step 6* with:

Step 1: We calculate $\overline{R_{IT-HWI}}(N)$ in (10) and record the results from $N = 10$ to $N = 100$.

Step 3: We calculate $R_{IT-HWI}(N)$ in (9) from $N = 10$ to $N = 100$, and record the ACR which is averaged on 1000 Monte Carlo trials at each N .

Step 5: As κ_t and κ_r are generally unknown for the IRS controller, we are unable to gain the optimal IRS phase shifts from the solution of Problem (28) in practice. Instead, we optimize the IRS phase shifts without HWI and extract the θ^T in the $(N + 1)th$ row of \mathbf{X} . By substituting the IRS phase shifts in the θ^T into the Φ in $R_{\Phi,IT-HWI}(N)$ in (25), we obtain the ACR with IT-HWI which is averaged on 1000 Monte Carlo trials at each N .

Step 6: We obtain the theoretical average ACR by solving Problem (28) at each N .

The average ACRs as functions of N with or without IT-HWI from $N = 10$ to $N = 100$ are presented in Figure 4. Figure 4 includes one main figure on the left and one subfigure on the right. The main figure displays the gaps between the lines without HWI and those with IT-HWI, while the subfigure describes the details of the theoretical and experimental results with IT-HWI. Figure 4 demonstrates that: First, the experimental results become higher than the theoretical ones as N increases, because we calculate the expectation of $P|\alpha \mathbf{g}_{IU}^T \Theta_{EGSI} + h_{SU}|^2$ inside $\log_2\{\cdot\}$ instead of the expectation of the ACR itself when deriving $\overline{R_{IT-HWI}}(N)$. Second, the average ACRs with IT-HWI are significantly lower than those without HWI, which indicates that the IT-HWI has great impact on the average ACR, and the transceiver HWI has even more effect on the average ACR than I-HWI. Third, the average ACRs with the optimized IRS phase shifts are higher than those with $\theta_i = -(\varphi_{IU,i} + \varphi_{SI,i})$, but are conspicuously reduced by the IT-HWI. This result indicates that $\theta_i = -(\varphi_{IU,i} + \varphi_{SI,i})$ is not the optimal phase shift as it does not take h_{SU} into account, and the average ACR is limited by the IT-HWI to a large extent.

The above simulation results validate the theoretical analyses in Section III and Section IV. Moreover, the proportionality factors of the transceiver HWI (κ_t and κ_r) will also influence the average ACR when there exists IT-HWI. Hence, we would numerically discuss on the average ACR in relation to κ , which is defined by $\kappa = \kappa_t + \kappa_r$, and compare the average ACR with that of the DF relay assisted system in the presence of IT-HWI.

D. Comparisons with Single-antenna DF Relay

In order to verify the theoretical results in Section V, we would numerically compare the average ACR with that of the conventional single-antenna DF relay assisted system in the presence of IT-HWI. The mathematical expression of the ACR of the single-antenna DF relay assisted system is different under two conditions, which are decided by μ_{SI} , μ_{IU} , μ_{SU} and $\kappa_t + \kappa_r$.

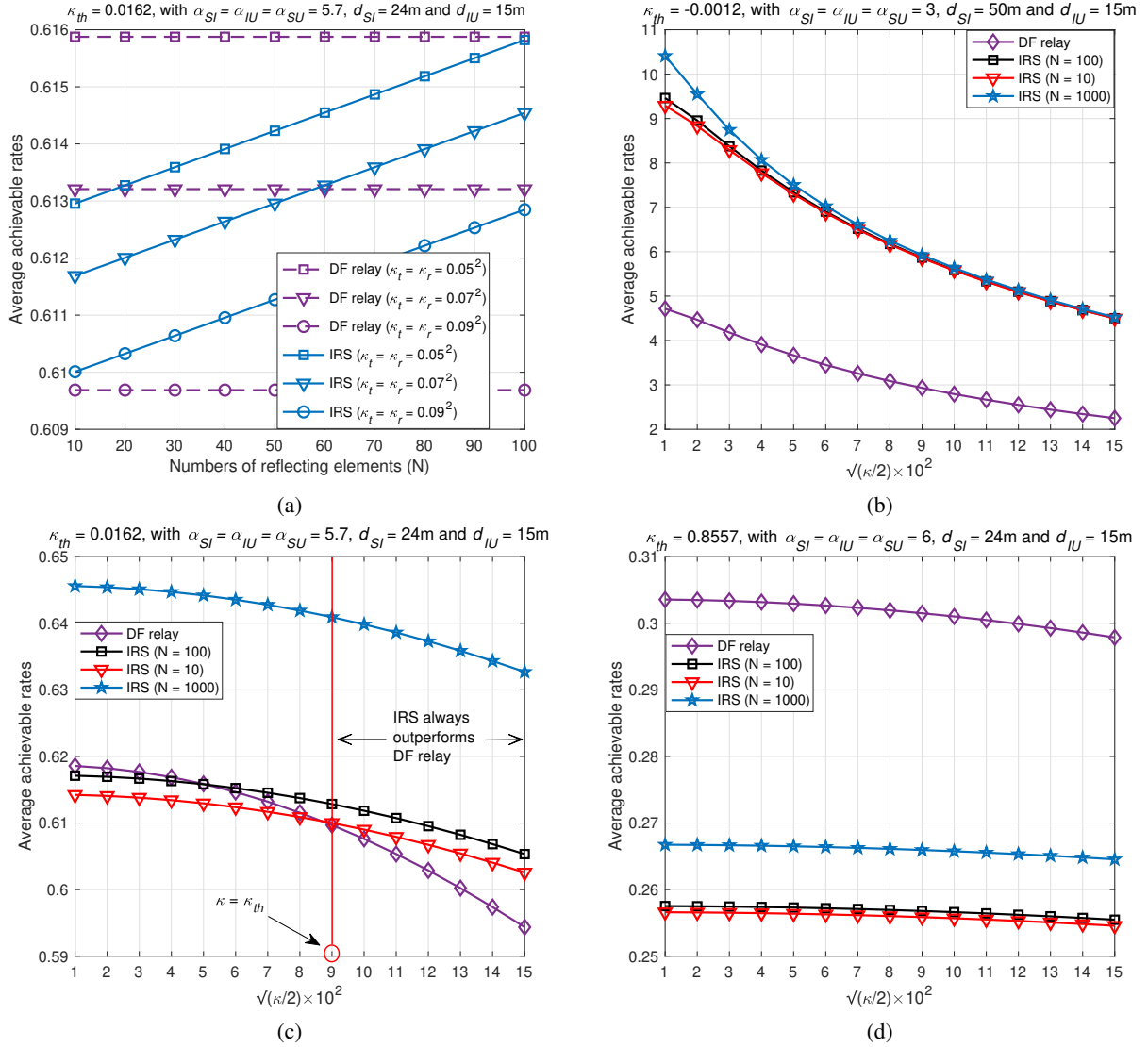
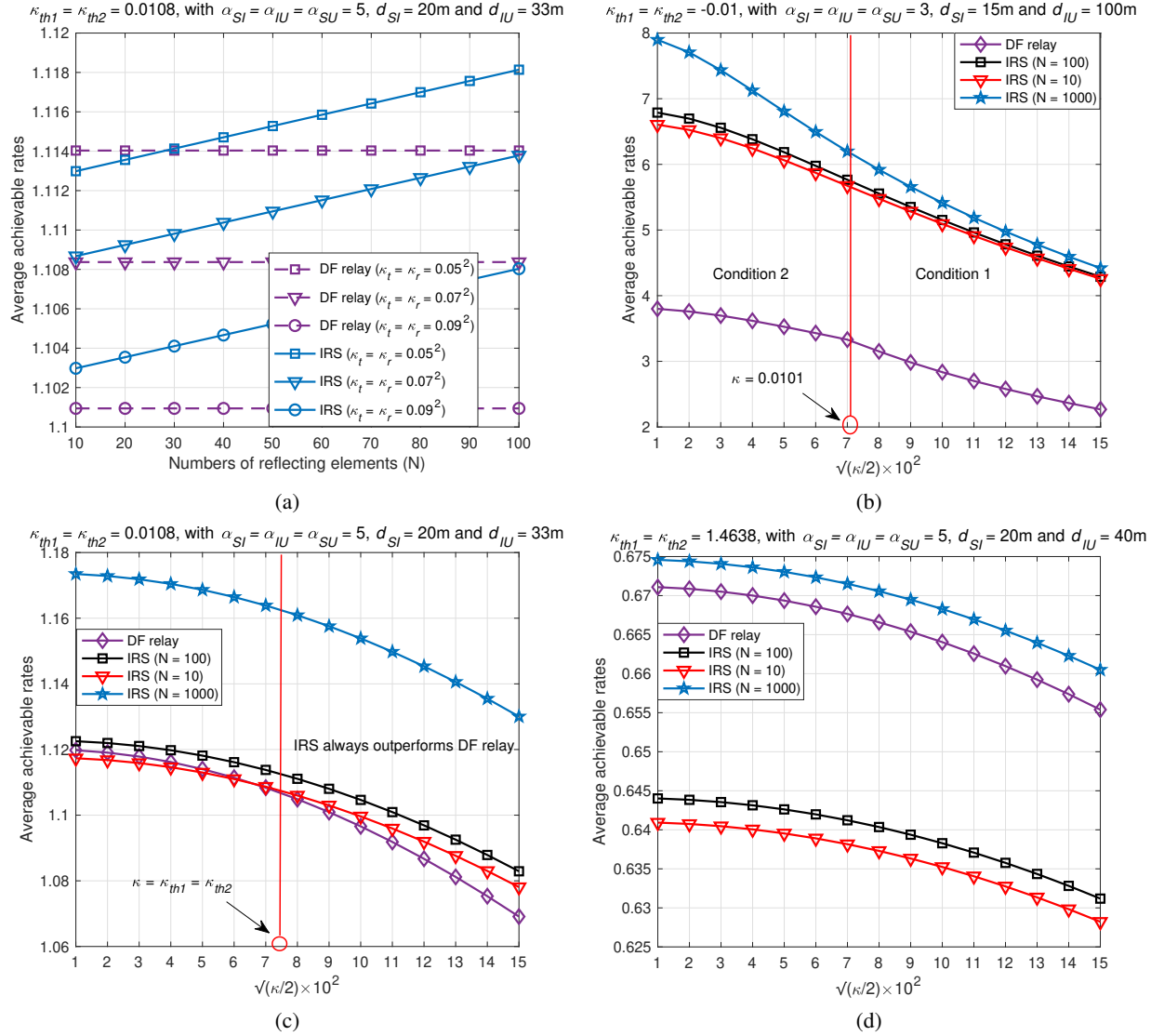


Fig. 5: Comparisons with DF relay under Condition 1. The abscissas in (b), (c) and (d) are defined by $\sqrt{\kappa/2} \times 10^2$ instead of κ_t or κ_r for integer counting, where $\kappa = \kappa_t + \kappa_r$ and $\kappa_t = \kappa_r$. (a) Average ACRs as functions of N . The parameters are set to be $d_{SI} = 24$ m, $d_{IU} = 15$ m and $\alpha_{SI} = \alpha_{IU} = \alpha_{SU} = 5.7$ for meeting Condition 1 and making κ_{th} a small positive number ($\kappa_{th} = 0.0162$), so that both $\kappa > \kappa_{th}$ and $\kappa < \kappa_{th}$ can be observed. (b) Average ACRs as functions of $\sqrt{\kappa/2} \times 10^2$. The parameters are set to be $d_{SI} = 50$ m, $d_{IU} = 15$ m and $\alpha_{SI} = \alpha_{IU} = \alpha_{SU} = 3$ for meeting Condition 1 and making κ_{th} a negative number ($\kappa_{th} = -0.0012$), so that κ can be always higher than κ_{th} . (c) Average ACRs as functions of $\sqrt{\kappa/2} \times 10^2$. The parameters are set to be $d_{SI} = 24$ m, $d_{IU} = 15$ m and $\alpha_{SI} = \alpha_{IU} = \alpha_{SU} = 5.7$ for meeting Condition 1 and making κ_{th} a small positive number ($\kappa_{th} = 0.0162$), so that the regions of $\kappa > \kappa_{th}$ and $\kappa < \kappa_{th}$ can be observed separately. The vertical red line stands for $\kappa = \kappa_{th}$, which is the demarcation of the two regions. (d) Average ACRs as functions of $\sqrt{\kappa/2} \times 10^2$. The parameters are set to be $d_{SI} = 24$ m, $d_{IU} = 15$ m and $\alpha_{SI} = \alpha_{IU} = \alpha_{SU} = 6$ for meeting Condition 1 and making κ_{th} a positive number ($\kappa_{th} = 0.8557$) which is relatively larger than κ_{th} in (c), so that $\kappa < \kappa_{th}$ when $1 < \sqrt{\kappa/2} \times 10^2 < 15$ and IRS cannot surpass DF relay when N is not large enough.

if $P_1 = P_2 = P$. Under each condition, N should exceed a certain value to guarantee that the IRS can surpass single-antenna DF relay on the average ACR. Moreover, whether the IRS can



always outperform single-antenna DF relay, is decided by whether $\kappa_t + \kappa_r$ is higher than κ_{th} under *Condition 1* or κ_{th1} under *Condition 2*, or lower than κ_{th2} under *Condition 2*. The κ_{th} , κ_{th1} and κ_{th2} are determined by S_{SI} , S_{IU} and S_{SU} , which are further determined by μ_{SI} , μ_{IU} and μ_{SU} if P and σ_w^2 are set fixed. In the parameter setting, μ_{SI} , μ_{IU} and μ_{SU} are defined in relation to the path loss exponents and the distances, which can be altered to change the conditions as well as κ_{th} , κ_{th1} and κ_{th2} . Accordingly, we would set different path loss exponents and distances to observe the comparisons under different conditions.

Comparisons under *Condition 1* are depicted in Figure 5. The average ACRs labelled with "IRS" and "DF relay" are obtained from (10) and (32), respectively. During the parameter setting, $d_{SI} > d_{IU}$ should be satisfied to ensure that the comparisons are made under *Condition 1*. First, the average ACRs as functions of N are described in Figure 5 (a). The parameters are set to be $d_{SI} = 24$ m, $d_{IU} = 15$ m and $\alpha_{SI} = \alpha_{IU} = \alpha_{SU} = 5.7$, as these configurations are examples that lead to small positive κ_{th} ($\kappa_{th} = 0.0162$), so that it is possible to observe both $\kappa > \kappa_{th}$ and $\kappa < \kappa_{th}$ when $10 < N < 100$. $\kappa_t = \kappa_r = 0.05^2$, 0.07^2 and 0.09^2 are selected for investigations according to [22] ($0 \leq \kappa_t = \kappa_r \leq 0.15^2$ in [22]). Figure 5 (a) demonstrates that when $\kappa_t = \kappa_r = 0.05^2$ or 0.07^2 , the IRS cannot surpass single-antenna DF relay when N is below a certain value (the intersection point of the solid line and the dashed line), but performs better when N exceeds the value, which is testified by (40). When $\kappa_t = \kappa_r = 0.09^2$, the IRS always outperforms single-antenna DF relay when $10 < N < 100$, because $\kappa_t + \kappa_r$ satisfies $\kappa_t + \kappa_r \geq \kappa_{th}$. Second, the average ACRs as functions of $\sqrt{\kappa/2} \times 10^2$ are described in Figure 5 (b), (c) and (d). The observation interval is bounded by $1 < \sqrt{\kappa/2} \times 10^2 < 15$ according to [22], where κ_t and κ_r are set within $(0, 0.15^2)$. In Figure 5 (b), the parameters are set to be $d_{SI} = 50$ m, $d_{IU} = 15$ m and $\alpha_{SI} = \alpha_{IU} = \alpha_{SU} = 3$, as these configurations are examples that result in negative κ_{th} ($\kappa_{th} = -0.0012$), so that the IRS can always surpass single-antenna DF relay according to **Lemma 5**. Figure 5 (b) indicates that the IRS performs better than single-antenna DF relay for all $1 < \sqrt{\kappa/2} \times 10^2 < 15$ when $N = 10, 100$ and 1000 , which verifies **Lemma 5** under these parameters. In Figure 5 (c), the parameters are set as same as those in Figure 5 (a), so that both $\kappa > \kappa_{th}$ and $\kappa < \kappa_{th}$ can be observed. Figure 5 (c) shows that the IRS conditionally outperforms single-antenna DF relay when $N = 10$ and 100 , and significantly performs better when $N = 1000$. The intersection point of the curves labelled with "IRS ($N = 10$)" and "DF relay" is close to $\kappa = \kappa_{th} = 0.0162$ (derived from $\sqrt{\kappa/2} \times 10^2 = 9$). At the right side of this point, the IRS with even quite a small N is able to surpass single-antenna DF relay, because $\kappa > \kappa_{th}$ allows the IRS to perform better for all $N > 0$. In Figure 5 (d), the parameters are set to be $d_{SI} = 24$ m, $d_{IU} = 15$ m and $\alpha_{SI} = \alpha_{IU} = \alpha_{SU} = 6$, as these configurations are examples that result in positive κ_{th} ($\kappa_{th} = 0.8557$), which is larger than the one in Figure 5 (c) and also larger than $\kappa = 0.045$ (derived from $\sqrt{\kappa/2} \times 10^2 = 15$), so that

there is $\kappa < \kappa_{th}$ when $1 < \sqrt{\kappa/2} \times 10^2 < 15$. Figure 5 (d) illustrates that when $N \leq 1000$, the IRS cannot outperform single-antenna DF relay because N is not large enough, specifically still lower than the value derived from (40).

These comparisons are made to view how large the IRS should become to surpass single-antenna DF relay and what κ can make the IRS always perform better. Taken together, Figure 5 demonstrates that the IRS can outperform single-antenna DF relay only when N is larger than a certain value if $\kappa < \kappa_{th}$, and can always perform better for all $N > 0$ if $\kappa > \kappa_{th}$. The number of N indicated by the intersection point is consistent with that derived from (40). Therefore, the above numerical results confirm **Theorem 3** and **Lemma 5** under *Condition 1*.

Comparisons under *Condition 2* are depicted in Figure 6. During the parameter setting, $d_{SI} < d_{IU}$ should be satisfied to ensure that the comparisons are made under *Condition 2*. In Figure 6 (a), (b), (c) and (d), the parameters are set to be $d_{SI} = 20$ m, $d_{IU} = 33$ m and $\alpha_{SI} = \alpha_{IU} = \alpha_{SU} = 5$, $d_{SI} = 15$ m, $d_{IU} = 100$ m and $\alpha_{SI} = \alpha_{IU} = \alpha_{SU} = 3$, $d_{SI} = 20$ m, $d_{IU} = 33$ m and $\alpha_{SI} = \alpha_{IU} = \alpha_{SU} = 5$, $d_{SI} = 20$ m, $d_{IU} = 40$ m and $\alpha_{SI} = \alpha_{IU} = \alpha_{SU} = 5$, which cause $\kappa_{th1} = \kappa_{th2} = 0.0108, -0.01, 0.0108$ and 1.4638 , respectively. There are three major distinctions between the results in Figure 6 and those in Figure 5: 1) A knee point, indicated by the vertical red line, on the curve labelled with "DF relay" can be observed In Figure 6 (b). This point locates on $\kappa = 0.0101$, whose left side involves the comparisons under *Condition 2* while the right side includes the comparisons under *Condition 1*. This phenomenon occurs because *Condition 2* relies on one more judgement expressed as (39) in **Lemma 4**. Only when $\kappa_t + \kappa_r$ satisfies (39) will the condition turn into *Condition 2*. The knee point is proved to be consistent with the value derived from the right-side expression in (39). 2) Figure 6 (c) shows that $\kappa > \kappa_{th1}$ is the requirement for the IRS to always outperform single-antenna DF relay because $1 + \frac{1}{S_{IU}} - \frac{1}{S_{SU}} > 0$, which numerically validates (42). 3) Figure 6 (d) demonstrates that the IRS can surpass single-antenna DF relay when $N = 1000$, because $N = 1000$ satisfies (40) under this parameter setting. Taken together, the above results confirm **Theorem 3** and **Lemma 5** under *Condition 2*.

E. Comparisons with Multi-antenna DF Relay

We would also make numerical comparisons with the multi-antenna DF relay assisted system, where we consider that the DF relay is also equipped with N antennas.

Figure 7 (a) depicts the average ACRs as functions of N when $\alpha_{SI} = \alpha_{IU} = \alpha_{SU} = 3$, $d_{SI} = 50$ m and $d_{IU} = 15$ m. Results in Figure 7 (a) demonstrate that under this parameter setting, the IRS performs better than multi-antenna DF relay from $N = 1$ to $N = 100$. Both the performances of the IRS and the multi-antenna DF relay degrade as κ_t and κ_r increase, which indicates that the transceiver HWI has impact on the performances. Figure 7 (b) depicts the average ACRs as functions of N when $\alpha_{SI} = \alpha_{IU} = \alpha_{SU} = 4.1$, $d_{SI} = 50$ m and $d_{IU} = 15$ m.

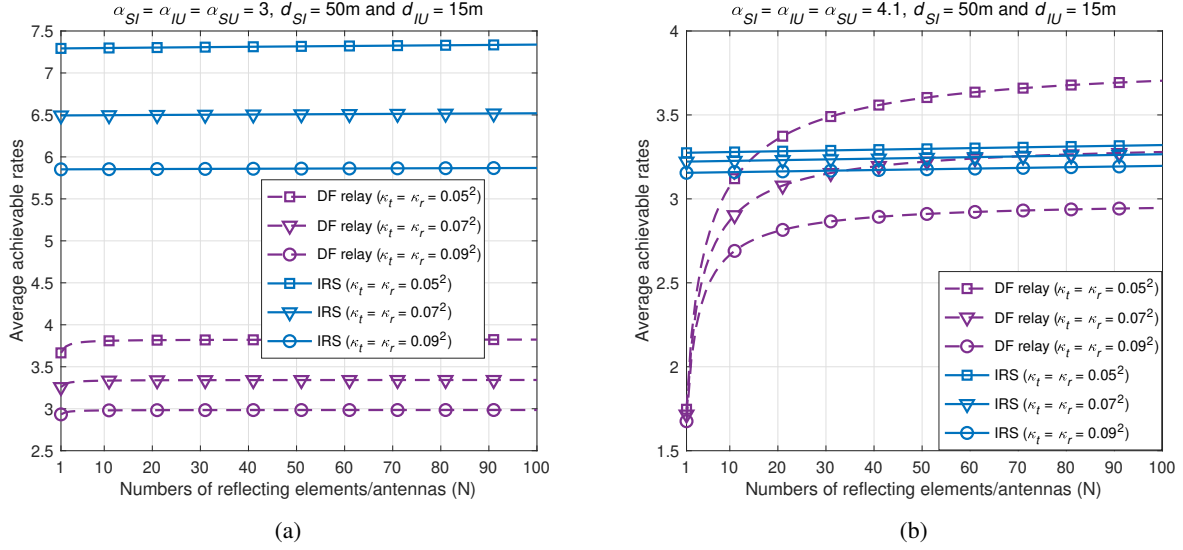


Fig. 7: Comparisons with multi-antenna DF relay on the average ACRs as functions of N . (a) The parameters are set to be $d_{SI} = 50$ m, $d_{IU} = 15$ m and $\alpha_{SI} = \alpha_{IU} = \alpha_{SU} = 3$. (b) The parameters are set to be $d_{SI} = 50$ m, $d_{IU} = 15$ m and $\alpha_{SI} = \alpha_{IU} = \alpha_{SU} = 4.1$.

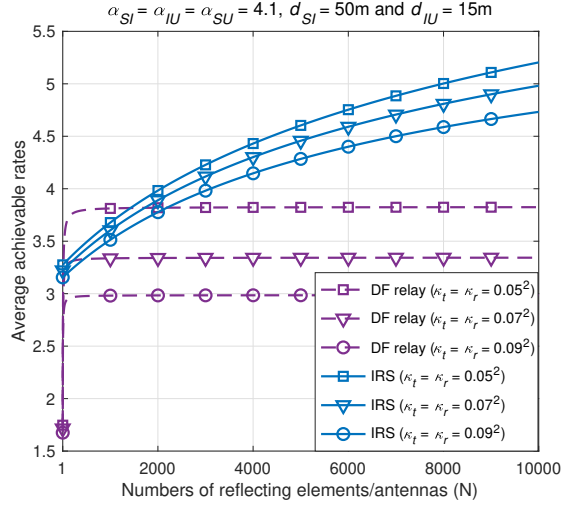


Fig. 8: Comparisons at very large N with multi-antenna DF relay on the average ACRs as functions of N . The parameters are set to be $d_{SI} = 50$ m, $d_{IU} = 15$ m and $\alpha_{SI} = \alpha_{IU} = \alpha_{SU} = 4.1$.

It is indicated in Figure 7 (b) that when $N < 15$, the IRS outperforms multi-antenna DF relay when $\kappa_t = \kappa_r = 0.05^2$, 0.07^2 or 0.09^2 . The average ACRs of the multi-antenna DF relay assisted system increase faster than those of the IRS-aided system when $N < 30$, but tend to be stable when $N > 30$. As N grows larger within $[1, 100]$, the multi-antenna DF relay can surpass IRS when $\kappa_t = \kappa_r = 0.05^2$, but cannot when $\kappa_t = \kappa_r = 0.07^2$ or 0.09^2 . As κ_t and κ_r increase, the multi-antenna DF relay suffers from more serious performance degradations than

the IRS, which indicates that the transceiver HWI has more influences on the multi-antenna DF relay than on the IRS. However, it cannot be concluded yet from Figure 7 (b) that the IRS cannot perform better when $N > 15$ and $\kappa_t = \kappa_r = 0.05^2$, because the observation interval is limited by $N \leq 100$. Hence, for investigating whether the IRS has opportunities to surpass multi-antenna DF relay with larger N , it is necessary to expand the observation range of N as depicted in Figure 8, where N is between $N = 1$ and $N = 10000$. Figure 8 demonstrates that the average ACRs of the multi-antenna DF relay assisted system increase rapidly as N grows at the beginning of the interval, but increase slowly when N is very large, while the average ACRs of the IRS-aided system show steady growth within the entire observation range. Although the multi-antenna DF relay is possible to beat IRS when $N < 2000$, the IRS can still perform better as N is large enough. Although it might not be realistic for the IRS and the multi-antenna DF relay to be equipped with such a large number of reflecting elements and antennas in practical implementations, these results confirm the possibility that the IRS with a very large number of reflecting elements can outperform multi-antenna DF relay with the same number of antennas.

VII. CONCLUSION

In this article, in order to evaluate the performance of the IRS in consideration of non-ideal hardware, we analyse the ACR of the IRS-aided wireless communication system and optimize the IRS phase shifts in the presence of HWI. Moreover, we compare the performance of the IRS with that of the conventional DF relay to investigate whether the IRS has advantages in improving the ACR over the traditional DF relay when there exists HWI. Results illustrate that 1) the average ACR of the IRS-aided system with HWI increases as the number of the reflecting units grows, 2) the HWI reduces the ACR of both the IRS-aided system and the DF relay assisted system, and 3) the IRS can surpass DF relay in the presence of HWI when the number of the reflecting units is large enough. Consequently, the IRS is proved to be still an effective facility for data transmission enhancement in the future communication networks with non-ideal hardware in the real world.

APPENDIX A

PROOF OF THEOREM 1

In Appendix A, we would prove **Theorem 1** in Section III. Let \mathbf{G}_{IU} and \mathbf{v}_E be defined by $\mathbf{G}_{IU} = \text{diag}(\mathbf{g}_{IU}) = \sqrt{\mu_{IU}}\mathbf{I}_N$ and $\mathbf{v}_E = (e^{j\theta_{E1}}, e^{j\theta_{E2}}, \dots, e^{j\theta_{EN}})^T$. Because $\mathbf{v}_E^T \mathbf{G}_{IU} = \mathbf{g}_{IU}^T \boldsymbol{\Theta}_E$,

from (4) we obtain

$$\begin{aligned}
 R_{I-HWI}(N) &= \log_2 \left[1 + \frac{P \left(\alpha^2 \mathbf{g}_{SI}^T \mathbf{G}_{IU}^T \mathbf{v}_E^* \mathbf{v}_E^T \mathbf{G}_{IU} \mathbf{g}_{SI} + \alpha \mathbf{g}_{SI}^T \mathbf{G}_{IU}^T \mathbf{v}_E^* h_{SU} + \alpha h_{SU}^* \mathbf{v}_E^T \mathbf{G}_{IU} \mathbf{g}_{SI} + \|h_{SU}\|_2^2 \right)}{\sigma_w^2} \right] \\
 &= \log_2 \left\{ 1 + \frac{P \left[\alpha^2 \mu_{IU} \mu_{SI} \text{tr}(\mathbf{v}_E^T \mathbf{\Gamma}_N \mathbf{v}_E^*) + \alpha \sqrt{\mu_{IU} \mu_{SI} \mu_{SU}} \sum_{i=1}^N (e^{j(\varphi_{SU} + \theta_{Ei})} + e^{-j(\varphi_{SU} + \theta_{Ei})}) + \|h_{SU}\|_2^2 \right]}{\sigma_w^2} \right\}
 \end{aligned} \tag{43}$$

We can expand $\text{tr}(\mathbf{v}_E^T \mathbf{\Gamma}_N \mathbf{v}_E^*)$ in (43) into

$$\begin{aligned}
 \text{tr}(\mathbf{v}_E^T \mathbf{\Gamma}_N \mathbf{v}_E^*) &= N + \sum_{i \neq 1}^N e^{j(\theta_{E1} - \theta_{Ei})} + \sum_{i \neq 2}^N e^{j(\theta_{E2} - \theta_{Ei})} + \dots + \sum_{i \neq N-1}^N e^{j(\theta_{E(N-1)} - \theta_{Ei})} + \sum_{i \neq N}^N e^{j(\theta_{EN} - \theta_{Ei})} \\
 &= N + 2 \sum_{i=2}^N \cos(\theta_{E1} - \theta_{Ei}) + 2 \sum_{i=3}^N \cos(\theta_{E2} - \theta_{Ei}) + \dots + 2 \sum_{i=N}^N \cos(\theta_{E(N-1)} - \theta_{Ei}) \\
 &= N + \mathbf{1M1}^T
 \end{aligned} \tag{44}$$

where the matrix \mathbf{M} is expressed as

$$\mathbf{M} = \begin{pmatrix} 2 \cos(\theta_{E1} - \theta_{E2}) & 2 \cos(\theta_{E2} - \theta_{E3}) & \dots & 2 \cos(\theta_{E(N-1)} - \theta_{EN}) \\ 2 \cos(\theta_{E1} - \theta_{E3}) & 2 \cos(\theta_{E2} - \theta_{E4}) & \dots & 0 \\ \vdots & \vdots & \ddots & \vdots \\ 2 \cos(\theta_{E1} - \theta_{E(N-1)}) & 2 \cos(\theta_{E2} - \theta_{EN}) & 0 & 0 \\ 2 \cos(\theta_{E1} - \theta_{EN}) & 0 & 0 & 0 \end{pmatrix} \tag{45}$$

We can also utilize Euler formula to expand $\sum_{i=1}^N (e^{j(\varphi_{SU} + \theta_{Ei})} + e^{-j(\varphi_{SU} + \theta_{Ei})})$ and then obtain $\sum_{i=1}^N (e^{j(\varphi_{SU} + \theta_{Ei})} + e^{-j(\varphi_{SU} + \theta_{Ei})}) = 2 \sum_{i=1}^N \cos(\varphi_{SU} + \theta_{Ei})$.

As θ_{Ei} , for $i = 1, 2, \dots, N$, are random variables which are uniformly distributed on $[-\pi/2, \pi/2]$, we should calculate the expectations of $2 \sum_{i=1}^N \cos(\varphi_{SU} + \theta_{Ei})$ and $\text{tr}(\mathbf{v}_E^T \mathbf{\Gamma}_N \mathbf{v}_E^*)$ in order to obtain a statistical average ACR. First, we calculate $\mathbb{E}_{\theta_{Ei}} \left[2 \sum_{i=1}^N \cos(\varphi_{SU} + \theta_{Ei}) \right]$ and have

$$\begin{aligned}
 \mathbb{E}_{\theta_{Ei}} \left[2 \sum_{i=1}^N \cos(\varphi_{SU} + \theta_{Ei}) \right] &= 2 \mathbb{E}_{\theta_{Ei}} \left[\sum_{i=1}^N \cos \varphi_{SU} \cos \theta_{Ei} - \sum_{i=1}^N \sin \varphi_{SU} \sin \theta_{Ei} \right] \\
 &= 2N \cos \varphi_{SU} \int_{-\pi/2}^{\pi/2} f(\theta_{Ei}) \cos \theta_{Ei} d\theta_{Ei} - 2N \sin \varphi_{SU} \int_{-\pi/2}^{\pi/2} f(\theta_{Ei}) \sin \theta_{Ei} d\theta_{Ei} \\
 &= \frac{4}{\pi} N \cos \varphi_{SU}
 \end{aligned} \tag{46}$$

where $f(\theta_{Ei}) = 1/\pi$ is the probability density function of variable θ_{Ei} .

Subsequently, we calculate $\mathbb{E}_{\theta_{Ei}} [\text{tr}(\mathbf{v}_E^T \mathbf{\Gamma}_N \mathbf{v}_E^*)] = N + \mathbb{E}_{\theta_{Ei}} [\mathbf{1M1}^T]$. It is notable that the elements in \mathbf{M} are either 0, or $2 \cos(\theta_{Ei} - \theta_{Ej})$ for $i < j$. Therefore, let $\Delta\theta$ be defined by $\Delta\theta = \theta_{Ei} - \theta_{Ej}$. Because θ_{Ei} obeys uniform distribution on $[-\pi/2, \pi/2]$, $\Delta\theta$ obeys triangular

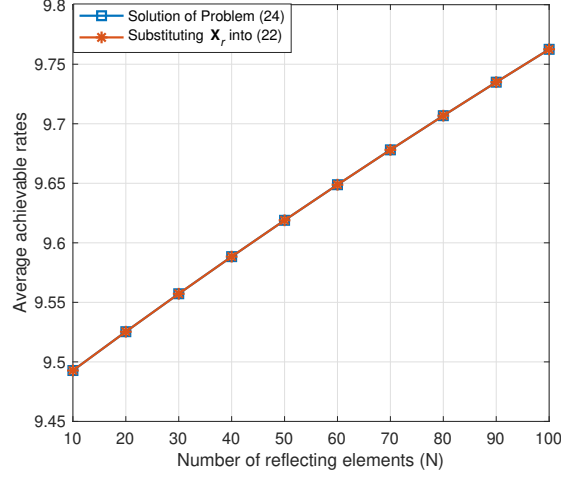


Fig. 9: Numerical test of the optimality of θ^T in \mathbf{X} . The line marked with "□" represents the average ACR derived by solving Problem (24). The line marked with "*" represents $\overline{R}_{\theta, I-HWI}(N)$ in (22) with \mathbf{X}_r .

distribution on $[-\pi, \pi]$ whose probability density function is expressed as

$$f(\Delta\theta) = \begin{cases} \frac{1}{\pi^2}\Delta\theta + \frac{1}{\pi}, & \Delta\theta \in [-\pi, 0] \\ -\frac{1}{\pi^2}\Delta\theta + \frac{1}{\pi}, & \Delta\theta \in [0, \pi] \end{cases} \quad (47)$$

Thus, we have

$$\begin{aligned} N + \mathbb{E}_{\theta_{Ei}} [\mathbf{1M}\mathbf{1}^T] &= N + \mathbb{E}_{\theta_{Ei}} \left[2 \sum_{i < j}^N \cos(\theta_{Ei} - \theta_{Ej}) \right] \\ &= N + N(N-1) \left[\int_{-\pi}^0 \left(\frac{1}{\pi^2}\Delta\theta + \frac{1}{\pi} \right) \cos(\Delta\theta) d\Delta\theta + \int_0^{\pi} \left(-\frac{1}{\pi^2}\Delta\theta + \frac{1}{\pi} \right) \cos(\Delta\theta) d\Delta\theta \right] \\ &= N \end{aligned} \quad (48)$$

By substituting (46) and (48) into (43), we finally prove **Theorem 1**.

APPENDIX B

NUMERICAL OPTIMALITY TEST FOR θ^T IN THE \mathbf{X}

In Appendix B, we would numerically test the optimality of θ^T in the \mathbf{X} through the following two steps.

Step 1: We set the parameters as introduced in Section VI and solve Problem (24) by using CVX toolbox. We obtain the average ACR by substituting the SNR in the solution into (22).

Step 2: We extract θ^T from the $(N+1)th$ row of the \mathbf{X} in the solution of Problem (24), and utilize θ^T to reconstruct the \mathbf{X} according to (16). Let \mathbf{X}_r denote the reconstructed \mathbf{X} . We substitute \mathbf{X}_r into (22) and obtain the average ACR.

Figure 9 depicts the average ACRs from $N = 10$ to $N = 100$. The lines marked with "□" and "*" represent the average ACRs derived in *Step 1* and in *Step 2*, respectively. Results in Figure 9 show that the two lines coincide, which indicates that $\mathbf{X}_r = \mathbf{X}$. Moreover, in the simulations, we calculate the rank of \mathbf{X}_r and obtain $\text{rank}(\mathbf{X}_r) = 1$ at each N . Because \mathbf{X}_r is constructed by $\boldsymbol{\theta}^T$ in the $(N + 1)$ th row of the \mathbf{X} in the solution, $\boldsymbol{\theta}^T$ is testified to be the optimal IRS phase shift vector.

APPENDIX C

PROOF OF LEMMA 3

In Appendix C, we would prove **Lemma 3** in Section V. On the assumption that $\kappa_{r2} = \kappa_{r1} = \kappa_{rDF} = \kappa_r$ and $\kappa_{tDF} = \kappa_t$, according to $\mathfrak{A} < \mathfrak{B}$ we have

$$\frac{1}{\kappa_t + \kappa_r + \frac{\sigma_w^2}{P_1\mu_{SI}}} < \frac{1}{\kappa_t + \kappa_r + \frac{\sigma_w^2}{P_1\mu_{SU}}} + \frac{1}{\kappa_t + \kappa_r + \frac{\sigma_w^2}{P_2\mu_{IU}}} \quad (49)$$

Let κ be defined by $\kappa = \kappa_t + \kappa_r$. Then, from (49) we obtain

$$\kappa^2 + \frac{2\sigma_w^2}{P_1\mu_{SI}}\kappa + \frac{\mu_{SU}P_1\sigma_w^4 + \mu_{IU}P_2\sigma_w^4 - \mu_{SI}P_1\sigma_w^4}{P_1^2P_2\mu_{SI}\mu_{IU}\mu_{SU}} > 0 \quad (50)$$

It is notable that the left side of inequation (50) is a quadratic function of κ . For holding (50) for all $\kappa > 0$, there should be $\Delta = b^2 - 4ac < 0$, where $a = 1$, $b = \frac{2\sigma_w^2}{P_1\mu_{SI}}$ and $c = \frac{\mu_{SU}P_1\sigma_w^4 + \mu_{IU}P_2\sigma_w^4 - \mu_{SI}P_1\sigma_w^4}{P_1^2P_2\mu_{SI}\mu_{IU}\mu_{SU}}$. Subsequently, on the basis of $\Delta = b^2 - 4ac < 0$ we obtain $\frac{4\sigma_w^4(\mu_{IU}P_2 - \mu_{SI}P_1)(\mu_{SU} - \mu_{SI})}{P_1^2P_2\mu_{SI}^2\mu_{IU}\mu_{SU}} < 0$. Because $\frac{4\sigma_w^4}{P_1^2P_2\mu_{SI}^2\mu_{IU}\mu_{SU}} > 0$, we have

$$\begin{cases} \mu_{IU}P_2 - \mu_{SI}P_1 > 0 \\ \mu_{SU} - \mu_{SI} < 0 \end{cases} \quad \text{or} \quad \begin{cases} \mu_{IU}P_2 - \mu_{SI}P_1 < 0 \\ \mu_{SU} - \mu_{SI} > 0 \end{cases} \quad (51)$$

By simplifying (51), we finally prove **Lemma 3**.

APPENDIX D

PROOF OF LEMMA 4

In Appendix D, we would prove **Lemma 4** in Section V. Similar to the proof of **Lemma 3** in Appendix C, we should calculate

$$\frac{1}{\kappa_t + \kappa_r + \frac{\sigma_w^2}{P_1\mu_{SI}}} > \frac{1}{\kappa_t + \kappa_r + \frac{\sigma_w^2}{P_1\mu_{SU}}} + \frac{1}{\kappa_t + \kappa_r + \frac{\sigma_w^2}{P_2\mu_{IU}}} \quad (52)$$

and obtain

$$\kappa^2 + \frac{2\sigma_w^2}{P_1\mu_{SI}}\kappa + \frac{\mu_{SU}P_1\sigma_w^4 + \mu_{IU}P_2\sigma_w^4 - \mu_{SI}P_1\sigma_w^4}{P_1^2P_2\mu_{SI}\mu_{IU}\mu_{SU}} < 0 \quad (53)$$

where $\kappa = \kappa_t + \kappa_r$. For holding (53) when $\kappa > 0$, there should be $\Delta = b^2 - 4ac > 0$ and $\kappa < \frac{-b + \sqrt{b^2 - 4ac}}{2a}$, where a , b and c have been defined in Appendix C. Finally, we prove (37)

and (38) by calculating $\Delta = b^2 - 4ac > 0$, and prove (39) by simplifying $\kappa < \frac{-b + \sqrt{b^2 - 4ac}}{2a}$.

APPENDIX E

PROOF OF LEMMA 5

In Appendix E, we would prove **Lemma 5** in Section V. As $\alpha^2 \mu_{IU} \mu_{SI} + \frac{4\alpha}{\pi} \sqrt{\mu_{IU} \mu_{SI} \mu_{SU}} \cos(\varphi_{SU})$ in the denominator in (40) is supposed to be larger than zero, whether IRS can always surpass DF relay is determined by $\frac{\sigma_w^2(\xi-1)}{P[1-(\xi-1)(\kappa_t+\kappa_r)]} - \mu_{SU}$ in the numerator. We would provide the derivations under *Condition 1* and *Condition 2*, respectively, as follows:

A. Derivations under Condition 1

Under *Condition 1*, the IRS will always outperform DF relay when

$$\frac{\sigma_w^2(\xi_{C1}-1)}{P[1-(\xi_{C1}-1)(\kappa_t+\kappa_r)]} - \mu_{SU} < 0 \quad (54)$$

because N is identically larger than zero which will always make (40) true. Herein, under the assumption that $P_1 = P_2 = P$, from (54) we have $\frac{1}{\xi_{C1}-1-(\kappa_t+\kappa_r)} < \frac{P\mu_{SU}}{\sigma_w^2}$. It is notable that $\frac{1}{\xi_{C1}-1} - (\kappa_t + \kappa_r) = \frac{\xi_{C1}}{(\xi_{C1}-1)(\xi_{C1}+1)} + \frac{\sigma_w^2}{P\mu_{SI}} > 0$ because $\xi_{C1} = \sqrt{1 + \frac{1}{\kappa_t+\kappa_r + \frac{\sigma_w^2}{P_1\mu_{SI}}}} > 1$. Therefore, we have $\left[\frac{\xi_{C1}}{(\xi_{C1}-1)(\xi_{C1}+1)} + \frac{\sigma_w^2}{P\mu_{SI}} \right] \frac{P\mu_{SU}}{\sigma_w^2} > 1$, which can further be transformed into

$$\xi_{C1}^2 - \frac{1}{\left(1 - \frac{\mu_{SU}}{\mu_{SI}}\right) \frac{\sigma_w^2}{P\mu_{SU}}} \xi_{C1} - 1 < 0 \quad (55)$$

The left side of (55) is a quadratic function of ξ_{C1} . It is remarkable that $\Delta = b^2 - 4ac = \left[\frac{1}{\left(1 - \frac{\mu_{SU}}{\mu_{SI}}\right) \frac{\sigma_w^2}{P\mu_{SU}}} \right]^2 + 4 > 0$, which makes the quadratic function include two zero solutions, where $a = 1$, $c = -1$ and $b = -\frac{1}{\left(1 - \frac{\mu_{SU}}{\mu_{SI}}\right) \frac{\sigma_w^2}{P\mu_{SU}}}$. Thus, for holding (55), ξ_{C1} should satisfy $\xi_1 < \xi_{C1} < \xi_2$, where $\xi_1 = \frac{-b-\sqrt{\Delta}}{2a}$ and $\xi_2 = \frac{-b+\sqrt{\Delta}}{2a}$.

Because $-b < \sqrt{\Delta}$, we have $\xi_1 < 0$. Hence, the range of ξ_{C1} is only limited by $\xi_{C1} < \xi_2$. Finally, we extract $\kappa_t + \kappa_r$ from ξ_{C1} on the left side of $\xi_{C1} < \xi_2$ and obtain the result in (41).

B. Derivations under Condition 2

Under *Condition 2*, the IRS will always outperform DF relay when

$$\frac{\sigma_w^2(\xi_{C2}-1)}{P[1-(\xi_{C2}-1)(\kappa_t+\kappa_r)]} - \mu_{SU} < 0 \quad (56)$$

If $P_1 = P_2 = P$, we have $\frac{1}{\xi_{C2}-1-(\kappa_t+\kappa_r)} < \frac{P\mu_{SU}}{\sigma_w^2}$. Because $\xi_{C2} < \xi_{C1}$ (derived from $\mathfrak{B} < \mathfrak{A}$ in *Condition 2*), which leads to $\frac{1}{\xi_{C2}-1} - (\kappa_t + \kappa_r) > \frac{1}{\xi_{C1}-1} - (\kappa_t + \kappa_r) > 0$, we have

$\left[\frac{1}{\xi_{C2}-1} - (\kappa_t + \kappa_r)\right] \frac{P_{\mu_{SU}}}{\sigma_w^2} > 1$. Let κ , S_{SU} and S_{IU} be defined by $\kappa = \kappa_t + \kappa_r$, $S_{SU} = \frac{P_{\mu_{SU}}}{\sigma_w^2}$ and $S_{IU} = \frac{P_{\mu_{IU}}}{\sigma_w^2}$, respectively. We expand ξ_{C2} and transform $\left[\frac{1}{\xi_{C2}-1} - (\kappa_t + \kappa_r)\right] \frac{P_{\mu_{SU}}}{\sigma_w^2} > 1$ into

$$\left(1 + \frac{1}{S_{IU}} - \frac{1}{S_{SU}}\right) \kappa^2 + \left(\frac{1}{S_{SU}} + \frac{1}{S_{IU}} + \frac{2}{S_{SU}S_{IU}} - \frac{2}{S_{SU}^2}\right) \kappa + \frac{1}{S_{SU}S_{IU}} + \frac{1}{S_{SU}^2S_{IU}} - \frac{1}{S_{SU}^3} > 0 \quad (57)$$

Let a , b and c be defined by $a = 1 + \frac{1}{S_{IU}} - \frac{1}{S_{SU}}$, $b = \frac{1}{S_{SU}} + \frac{1}{S_{IU}} + \frac{2}{S_{SU}S_{IU}} - \frac{2}{S_{SU}^2}$ and $c = \frac{1}{S_{SU}S_{IU}} + \frac{1}{S_{SU}^2S_{IU}} - \frac{1}{S_{SU}^3}$, respectively, so that (57) can be written as $a\kappa^2 + b\kappa + c > 0$. We calculate the discriminant of $a\kappa^2 + b\kappa + c$ and obtain $\Delta = b^2 - 4ac = \left(\frac{1}{S_{SU}} - \frac{1}{S_{IU}}\right)^2 > 0$, which indicates that $a\kappa^2 + b\kappa + c$ has two zero solutions. Because *Condition 2* stipulates that $\mu_{SU} < \mu_{IU}$, we have $\frac{1}{S_{SU}} - \frac{1}{S_{IU}} > 0$, which results in $\sqrt{\Delta} = \frac{1}{S_{SU}} - \frac{1}{S_{IU}}$. Therefore, for holding (57), κ should satisfy $\kappa_1 < \kappa < \kappa_2$ if $a < 0$, or satisfy $\kappa < \kappa_1 \cup \kappa > \kappa_2$ if $a > 0$, where $\kappa_1 = \frac{-b-\sqrt{\Delta}}{2a} = -\frac{1}{S_{SU}}$ and $\kappa_2 = \frac{-b+\sqrt{\Delta}}{2a} = \frac{S_{IU}-S_{SU}^2-S_{SU}}{S_{SU}^2S_{IU}+S_{SU}^2-S_{SU}S_{IU}}$. Consequently, we obtain (42) and prove **Lemma 5** based on the aforementioned derivations.

REFERENCES

- [1] M. Agiwal, A. Roy and N. Saxena, Next generation 5G wireless networks: a comprehensive survey, *IEEE Communications Surveys & Tutorials*, vol. 18, no. 3, pp. 16171655, Third Quarter 2016.
- [2] W. Yan, X. Yuan and X. Kuai, "Passive beamforming and information transfer via large intelligent surface," *IEEE Wireless Communications Letters*, to be published. DOI: 10.1109/LWC.2019.2961670.
- [3] X. Lin and J. G. Andrews, "Connectivity of millimeter wave networks with multi-hop relaying," *IEEE Wireless Communications Letters*, vol. 4, no. 2, pp. 209212, Apr. 2015.
- [4] W. Sun and J. Liu, "2-to-M coordinated multipoint-based uplink transmission in ultra-dense cellular networks," *IEEE Transactions on Wireless Communications*, vol. 17, no. 12, pp. 83428356, Dec. 2018.
- [5] S. Hu, F. Rusek and O. Edfors, "Beyond massive MIMO: the potential of data transmission with large intelligent surfaces," *IEEE Transactions on Signal Processing*, vol. 66, no. 10, pp. 27462758, May. 2018.
- [6] S. Cheng, R. Wang, J. Wu, W. Zhang and Z. Fang, "Performance analysis and beamforming designs of MIMO AF relaying with hardware impairments," *IEEE Transactions on Vehicular Technology*, vol. 67, no. 7, pp. 62296243, Jul. 2018.
- [7] P. K. Sharma and P. K. Upadhyay, "Cognitive relaying with transceiver hardware impairments under interference constraints," *IEEE Communications Letters*, vol. 20, no. 4, pp. 820823, Apr. 2016.
- [8] X. Xia *et al.*, "Hardware impairments aware transceiver for full-duplex massive MIMO relaying," *IEEE Transactions on Signal Processing*, vol. 63, no. 24, pp. 65656580, Dec. 2015.
- [9] A. K. Mishra and P. Singh, "Performance analysis of opportunistic transmission in downlink cellular DF relay network with channel estimation error and RF impairments," *IEEE Transactions on Vehicular Technology*, vol. 67, no. 9, pp. 90219026, Sep. 2018.
- [10] . zdogan, E. Bjrnson and E. G. Larsson, "Intelligent reflecting surfaces: physics, propagation, and pathloss modeling," *IEEE Wireless Communications Letters*, to be published. DOI: 10.1109/LWC.2019.2960779.
- [11] Q. Wu and R. Zhang, "Beamforming optimization for intelligent reflecting surface with discrete phase shifts," in *Proc. 2019 IEEE International Conference on Acoustics, Speech and Signal Processing (ICASSP)*, Brighton, United Kingdom, May. 2019, pp. 78307833.
- [12] Z. He and X. Yuan, "Cascaded channel estimation for large intelligent metasurface assisted massive MIMO," *IEEE Wireless Communications Letters*, vol. 9, no. 2, pp. 210214, Feb. 2020.
- [13] Q. Wu and R. Zhang, "Intelligent reflecting surface enhanced wireless network via joint active and passive beamforming," *IEEE Transactions on Wireless Communications*, vol. 18, no. 11, pp. 53945409, Nov. 2019.

- [14] E. Basar, "Reconfigurable intelligent surface-based index modulation: a new beyond MIMO paradigm for 6G," *IEEE Transactions on Communications*, to be published. DOI: 10.1109/TCOMM.2020.2971486.
- [15] M. Cui, G. Zhang and R. Zhang, "Secure wireless communication via intelligent reflecting surface," *IEEE Wireless Communications Letters*, vol. 8, no. 5, pp. 14101414, Oct. 2019.
- [16] H. Shen *et al.*, "Secrecy rate maximization for intelligent reflecting surface assisted multi-antenna communications," *IEEE Communications Letters*, vol. 23, no. 9, pp. 14881492, Sep. 2019.
- [17] Q. Nadeem *et al.*, "Intelligent reflecting surface assisted wireless communication: modeling and channel estimation," Dec. 2019. [Online]. Available: arXiv:1906.02360v2.
- [18] E. Bjrnson, . zdogan and E. G. Larsson, "Intelligent reflecting surface versus decode-and-forward: how large surfaces are needed to beat relaying?" *IEEE Wireless Communications Letters*, vol. 9, no. 2, pp. 244248, Feb. 2020.
- [19] X. Zhang, M. Matthaiou, M. Coldrey and E. Bjrnson, "Impact of residual transmit RF impairments on training-Based MIMO systems," *IEEE Transactions on Communications*, vol. 63, no. 8, pp. 28992911, Aug. 2015.
- [20] K. Xu *et al.*, "Achievable rate of full-duplex massive MIMO relaying with hardware impairments," in *Proc. 2015 IEEE Pacific Rim Conference on Communications, Computers and Signal Processing (PACRIM)*, Victoria, BC, Canada, Aug. 2015, pp. 8489.
- [21] T. Schenk, *RF Imperfections in High-Rate Wireless Systems: Impact and Digital Compensation*. New York, NY, USA: Springer-Verlag, 2008.
- [22] E. Bjrnson, J. Hoydis, M. Kountouris and M. Debbah, "Massive MIMO systems with non-ideal hardware: energy efficiency, estimation, and capacity limits," *IEEE Transactions on Information Theory*, vol. 60, no. 11, pp. 71127139, Nov. 2014.
- [23] E. Bjrnson, P. Zetterberg, M. Bengtsson and B. Ottersten, "Capacity limits and multiplexing gains of MIMO channels with transceiver impairments," *IEEE Communications Letters*, vol. 17, no. 1, pp. 9194, Jan. 2013.
- [24] Q. Zhang, T. Q. S. Quek and S. Jin, "Scaling analysis for massive MIMO systems with hardware impairments in Rician fading," *IEEE Transactions on Wireless Communications*, vol. 17, no. 7, pp. 45364549, Jul. 2018.
- [25] S. Hu, F. Rusek and O. Edfors, "Capacity degradation with modeling hardware impairment in large intelligent surface," in *Proc. 2018 IEEE Global Communications Conference (GLOBECOM)*, Abu Dhabi, United Arab Emirates, United Arab Emirates, Dec. 2018, pp. 16.
- [26] M. A. Badiu and J. P. Coon, "Communication through a large reflecting surface with phase errors," *IEEE Wireless Communications Letters*, vol. 9, no. 2, pp. 184188, Feb. 2020.
- [27] B. Zheng and R. Zhang, "Intelligent reflecting surface-enhanced OFDM: channel estimation and reflection optimization," *IEEE Wireless Communications Letters*, to be published. DOI: 10.1109/LWC.2019.2961357.
- [28] A. Nemirovski and M. J. Todd, "Interior-point methods for optimization," *Acta Numerica*, vol. 17, pp. 191234, May. 2008.
- [29] J. N. Laneman, D. N. C. Tse, and G. W. Wornell, Cooperative diversity in wireless networks: Efficient protocols and outage behavior, *IEEE Transactions on Information Theory*, vol. 50, no. 12, pp. 30623080, Dec. 2004.